REVIEW ARTICLE
Yoshiki Niihori, Yuichi Negishi *et al.*
Triplet–triplet annihilation-based photon upconversion using nanoparticles and nanoclusters

10 YEARS ANNIVERSARY

REVIEW

Check for updates

Triplet–triplet annihilation-based photon upconversion using nanoparticles and nanoclusters

Yoshiki Niihori, [iD] *[a] Taiga Kosaka[b] and Yuichi Negishi [iD] *[abc]

The phenomenon of photon upconversion (UC), generating high-energy photons from low-energy photons, has attracted significant attention. In particular, triplet–triplet annihilation-based UC (TTA-UC) has been achieved by combining the excitation states of two types of molecules, called the sensitizer and emitter (or annihilator). With TTA-UC, it is possible to convert weak, incoherent near-infrared (NIR) light, which constitutes half of the solar radiation intensity, into ultraviolet and visible light that are suitable for the operation of light-responsive functional materials or devices such as solar cells and photocatalysts. Research on TTA-UC is being conducted worldwide, often employing materials with high intersystem crossing rates, such as metal porphyrins, as sensitizers. This review summarizes recent research and trends in triplet energy transfer and TTA-UC for semiconductor nanoparticles or nanocrystals with diameters in the nanometer range, also known as quantum dots, and for ligand-protected metal nanoclusters, which have even smaller well-defined sub-nanostructures. Concerning nanoparticles, transmitter ligands have been applied on the surface of the nanoparticles to efficiently transfer triplet excitons formed inside the nanoparticles to emitters. Applications are expanding to solid-state UC devices that convert NIR light to visible light. Additionally, there is active research in the development of sensitizers using more cost-effective and environmentally friendly elements. Regarding metal nanoclusters, methods have been established for the evaluation of excited states, deepening the understanding of luminescent properties and excited relaxation processes.

Wider impact

The imperative to acquire clean energy sources is underscored by the impacts of global warming. Solar radiation is an attractive energy source because it is abundantly available on Earth's surface; however, most materials and devices are driven by ultraviolet and visible light, leaving the near-infrared (NIR) sunlight untapped. Triple–triplet annihilation upconversion (TTA-UC) is an energy conversion technique that uses a combination of sensitizer and emitter molecules to convert the underutilized NIR light into visible light that is usable in devices. In particular, inorganic nanomaterials, such as semiconductor nanoparticles with sizes around a few nanometers and ligand-protected metal nanoclusters with precisely defined compositions, have been identified for their ability to sensitize the excited triplet states of emitter molecules. These inorganic nanomaterials, with tunable electronic states based on their size and composition, exhibit broad absorption bands in the NIR region. The application of these inorganic nanomaterials for highly efficient NIR upconversion is expected to improve the performance of solar harvesting devices, surpassing the TTA-UC capabilities of conventional organic sensitizers and maximizing the use of incoming solar rays.

1. Introduction

The Earth's surface receives approximately 0.1 W cm^{-2} of solar radiation, consisting mainly of ultraviolet (UV), visible, and near-infrared (NIR) light. Attempts to harness this abundant solar energy to enrich human life have a history dating back approximately 10,000 years with the invention of agriculture.[1] This effort continued through the advent of solar water heaters in ancient Greece and Rome and evolved into modern technologies that convert solar energy into electricity or chemical energy.

Since the Industrial Revolution, the deterioration of the environment due to the consumption of fossil fuels has sparked demand for the development of materials and energy sources with lower environmental impact. In particular,

[a] *Research Institute for Science and Technology, Tokyo University of Science, 1-3 Kagurazaka, Shinjuku-ku, Tokyo 162-8601, Japan. E-mail: niihori@rs.tus.ac.jp, negishi@rs.tus.ac.jp*

[b] *Graduate School of Science, Department of Chemistry, Tokyo University of Science, 1-3 Kagurazaka, Shinjuku-ku, Tokyo 162-8601, Japan*

[c] *Department of Applied Chemistry, Faculty of Science, Tokyo University of Science, 1-3 Kagurazaka, Shinjuku-ku, Tokyo 162-8601, Japan*

materials and devices that exploit solar energy, such as photocatalysts and solar cells, for driving material transformations or converting energy into electricity align with this goal. More efficient versions of these optical materials and devices are continually being developed. The mechanisms of these materials and devices start with the formation of electron-excited states, which requires UV and visible light with energies of several electron volts. However, approximately half of the solar radiation reaching the Earth's surface consists of lower-energy NIR light. Currently, efficiently creating electron-excited states from NIR light is challenging, and as a result, humanity has not developed the technology to fully harness the solar spectrum.

In recent years, the phenomenon of upconversion (UC) has garnered attention as a promising method to overcome this challenge. The conversion from low-energy states to high-energy states is known as UC, and in the context of light energy, it is referred to as photon UC. Various methods, such as the use of rare earth compounds and two-photon absorption, have been employed to achieve optical UC.[2–5] In particular, triplet–triplet annihilation-based photon UC (TTA-UC), which leverages the reactions between the excitation states of sensitizer and emitter molecules, has been proposed to convert weak incoherent NIR light from solar radiation into UV and visible light.[6,7]

While metalloporphyrins and other phosphorescent materials are representative sensitizers in TTA-UC, recent advancements have revealed the potential use of semiconductor quantum dots consisting of sizes ranging from several to tens of nanometers. More recently, the potential of ligand-protected metal nanoclusters composed of a finite number of noble metal atoms as sensitizers in TTA-UC has also been identified.

To date, numerous sensitizing molecules based on organic metal complexes have been developed for TTA-UC, and several reviews have been published.[8–14] Similarly, inorganic nanomaterials that are capable of interacting with light across a wide range of wavelengths have gained attention as sensitizing molecules. Theoretical discussions unique to nanomaterials, such as those regarding excitons and efficient energy transfer through triplet transmitters, have been established. In addition, Meinardi, Mongzzi, and their coworkers have also developed a detailed kinetic analysis method for systems consisting of transmitter-modified nanoparticle sensitizers and emitters.[15] However, comprehensive reviews focusing on their triplet sensitization and application to TTA-UC are scarce.[16]

This review compiles research on the performance of inorganic nanomaterials as sensitizers and their application to TTA-UC, ranging from nanoscale particles and nanocrystals to even smaller nanoclusters. Through this compilation, we aim to discuss the current understanding, challenges, and prospects for future research.

In Chapter 2, we first introduce the mechanism of TTA-UC and the physical quantities to be obtained. Subsequently, in Chapter 3, we discuss the triplet sensitization and TTA-UC performance of homogenous nanoparticles, core–shell nanoparticles, perovskite nanocrystals, and metal-free nanoparticles with sizes on the order of several nanometers. In Chapter 4, we extend our discussion to sub-nanometer-sized nanoclusters composed of noble metals, covering their triplet sensitization,

Yoshiki Niihori

Yoshiki Niihori is a Junior Associate Professor in Prof. Negishi group at Tokyo University of Science (TUS). He received a PhD degree in Chemistry (2014) from TUS under the supervision of Prof. Yuichi Negishi. Before the current position, he was employed as an Assistant Professor in Prof. Mitsui group at Rikkyo University. His research interests include the development of precise synthesis methods and characterization of photoexcited state for noble metal nanoclusters.

Taiga Kosaka

Taiga Kosaka is a master's course student in the Negishi group at TUS. He received a BSc (2023) in Chemistry from TUS. His research interests include the establishment of the methods for connecting metal clusters.

Yuichi Negishi

Yuichi Negishi is a Professor at the Department of Applied Chemistry at TUS. He received a PhD degree in Chemistry (2001) from Keio University under the supervision of Prof. Atsushi Nakajima. Before joining TUS in 2008, he was employed as an Assistant Professor at Keio University (Nakajima group) and the Institute for Molecular Science (Tsukuda group). His current research interests include the precise synthesis of stable and functionalized metal nanoclusters, metal nanocluster-connected structures, and covalent organic frameworks.

TTA-UC characteristics, and the excited states of the metal nanoclusters themselves. After summarizing the review in Chapter 5, we conclude the review by discussing future perspectives in Chapter 6. We hope that this review facilitates mutual understanding among researchers in the fields of UC and inorganic nanomaterials.

2. Fundamentals of TTA-UC

Mechanism of TTA-UC

TTA-UC is achieved using two types of molecules: the triplet sensitizer (Sen) and the emitter/annihilator (Em). The proposed mechanism is illustrated in Scheme 1. Initially, the sensitizer molecule in the ground (S_0) state (^{1}Sen) absorbs light, leading to the formation of the excited singlet (S_1) state (^{1}Sen*). Subsequently, through intersystem crossing (ISC), the long-lived excited triplet (T_1) state (^{3}Sen*) is generated. It should be noted that while this process provides an accurate description for general sensitizers represented by metalloporphyrin complexes and the inorganic nanoclusters to be introduced later, in the case of inorganic nanoparticles, an excited state of sensitizer (Sen*) characterized as a mixed state of the S_1 and T_1 states is formed. Consequently, the energy loss due to intersystem crossing (ISC) is minimized in inorganic nanoparticles. This persistent ^{3}Sen* or Sen* molecule sensitizes the T_1 state of the emitter molecule in the S_0 state (^{1}Em → ^{3}Em*) *via* Dexter-type triplet energy transfer (TET). Subsequently, triplet–triplet annihilation (TTA) occurs between the two ^{3}Em* molecules, resulting in one emitter transitioning to the S_0 state and the other to the S_1 state (^{1}Em*). Finally, the fluorescence (F) photon is emitted as UC fluorescence from ^{1}Em*. The emission spectrum of these UC photons exhibits a similar shape to the emission spectrum obtained when directly exciting the emitter. However, in the emission process of UC photons through TTA-UC, involving the T_1 state of the emitter, the UC is observed as delayed fluorescence, reflecting the T_1 lifetime of the emitter.[17]

In this manuscript, we primarily focus on solution-based systems involving molecules dissolved in a solvent. We denote the solution system consisting of the sensitizer and emitter as "Sen/Em." Additionally, we represent complexes where some of the protective ligands on the sensitizer surface are replaced with transmitter ligands (Trans) as "Sen:Trans" and further

denote solution systems combining this complex with the emitter as "Sen:Trans/Em."

Anti-Stokes Shift

In typical single-component fluorescent dyes, the emission peak is observed at a longer wavelength than the excitation wavelength. The energy difference between the absorption peak and the emission peak, expressed in units of cm^{-1} or eV, is known as the Stokes shift, providing information about the molecule's excited state. Conversely, in TTA-UC, the observed UC wavelength is shorter than the excitation photon wavelength (Fig. 1). The difference between the excitation photon energy and the UC photon energy, analogous to the Stokes shift, is referred to as the anti-Stokes shift (ΔE_{AS}) (Fig. 1), and is described as follows:
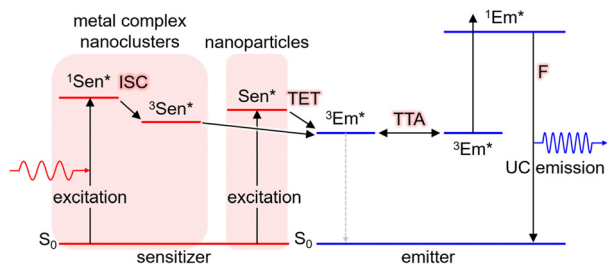
$$\Delta E_{AS} = \frac{1}{\lambda_{UC}} - \frac{1}{\lambda_{ex}}. \tag{1}$$

The estimation of λ_{UC} can vary in the literature, using the peak wavelength or centroid wavelength of the UC spectrum. TTA-UC experiments are often conducted under conditions where the concentrations of Sen and Em ([Sen] and [Em]) are in the range of several tens of μM to several tens of mM. Under such high concentrations, when using fluorescent dyes with small Stokes shifts, such as perylene or acene-based dyes as emitters, self-absorption, also known as self-quenching, occurs where the fluorescence peak near the 0–0 transition energy is absorbed by the emitter. Consequently, a decrease in ΔE_{AS} is observed. Therefore, the value of ΔE_{AS} depends on the sample concentration, sample form, and experimental setup, including the position of the excitation light irradiation.

UC efficiency

The UC efficiency (Φ_{UC}) is the ratio of the number of detected UC emitting photons to the number of absorbed photons, defined by the following equation:

$$\Phi_{UC} = \frac{\text{\# of detected UC emitting photon}}{\text{\# of absorbed photon}}. \tag{2}$$

Scheme 1 Scheme of TTA-UC in the Sen/Em system. Sen: sensitizer (metal complex, nanoclusters, or nanoparticles), Em: emitter, ISC: intersystem crossing, TET: triplet energy transfer, TTA: triplet–triplet annihilation.
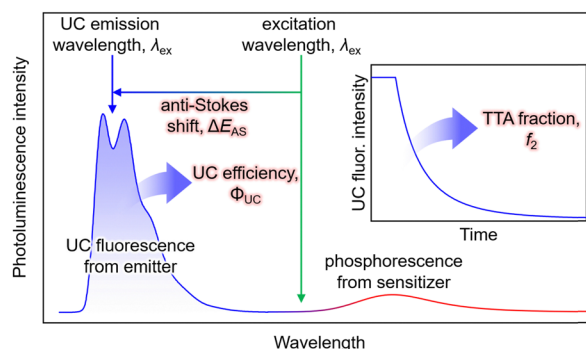

Fig. 1 Typical photoluminescence spectrum of a solution system consisting of sensitizer and emitter molecules (Sen/Em). In the inset, the decay of UC fluorescence intensity is depicted. Note that this spectrum and decay curve are just schematic, and were not obtained experimentally.

Similar to the conventional fluorescence quantum yield (Φ_F), Φ_{UC} can be experimentally evaluated using either a relative method with standard dyes or an absolute method employing an integrating sphere (Fig. 1).[18]

Because TTA-UC involves reactions within/between two excited-state molecules, Φ_{UC} can be expressed as the product of the quantum yields of each subprocess. There are various ways to express this, but we use the following unified expression:

$$\Phi_{UC} = \Phi_{ISC} \cdot \Phi_{TET} \cdot \Phi_{TTA} \cdot \Phi_F. \qquad (3)$$

Here, Φ_{ISC} is the ISC efficiency of the sensitizer molecule. Note that when the nanoparticles are used as the sensitizer, its excited state is a mixture of the S_1 and T_1 states. As a result, Φ_{ISC} of nanoparticles is often disregarded, $i.e.$ $\Phi_{ISC} \sim 1$ (100%). Φ_{TET} is the TET efficiency from $^3Sen^*$ or Sen^* to $^3Em^*$, Φ_{TTA} is the efficiency of generating $^1Em^*$ from two $^3Em^*$ molecules through TTA, and Φ_F is the fluorescence quantum yield of the emitter molecule. In the TTA process, one $^1Em^*$ molecule involved in fluorescence is generated from two $^3Em^*$ molecules. Therefore, the theoretical maximum value of Φ_{UC} is 0.5 (50%). In this case, the theoretical maximum value of Φ_{TTA} is also 0.5 (50%), whereas the theoretical maximum quantum yields of other subprocesses are 1 (100%). Note that the measured Φ_{UC} is multiplied by a factor of 2 in some studies, making the theoretical maximum value of Φ_{UC} and Φ_{TTA} 1 (100%). In this manuscript, the Φ_{UC} values multiplied by a factor of 2 are denoted as Φ'_{UC}:

$$\Phi'_{UC} = 2\Phi_{UC}. \qquad (4)$$

As mentioned later, experimentally obtained Φ_{UC} and Φ'_{UC} depend on the concentrations of the sensitizer and emitter, as well as the intensity of the excitation light.

Furthermore, several literatures discuss the consideration of the quenching effect of UC fluorescence due to the presence of high concentration of emitters (internal filter effect), termed Φ_{UCg}. This value is obtained experimentally by dividing Φ_{UC} by the optical outcoupling yield of the sample (Φ_{out}).[19]

$$\Phi_{UCg} = \frac{\Phi_{UCg}}{\Phi_{out}}. \qquad (5)$$

The Φ_{out} can be derived from transmittance spectrum of TTA-UC sample solution and fluorescence spectrum of low concentration solution of emitter excited under normal condition.

TET efficiency

For the Sen/Em system, determining the phosphorescence quenching of the sensitizer due to the addition of the emitter allows for the calculation of the TET efficiency (Φ_{TET}) through Stern–Volmer analysis, as depicted in Fig. 2. The relationship between the Stern–Volmer constant (K_{SV}) and Φ_{TET} is expressed as follows:[20]

$$\Phi_{TET} = \frac{K_{SV}[Em]}{1 + K_{SV}[Em]}. \qquad (6)$$

Thus, Φ_{TET} is a function of the emitter concentration [Em]. The rate constant k_{TET} for TET can be estimated by dividing K_{SV}
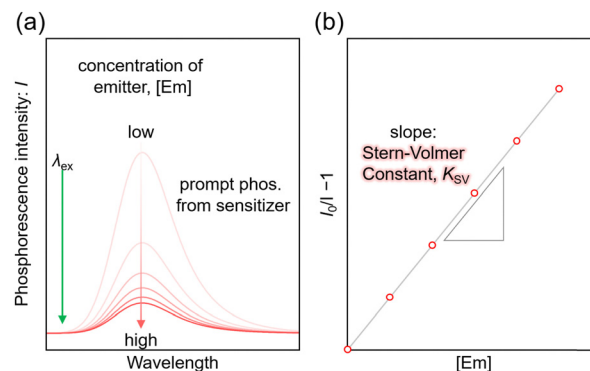

Fig. 2 (a) Phosphorescence spectra of the sensitizer as a function of emitter concentration and (b) Stern–Volmer plot in a solution system consisting of sensitizer and emitter (Sen/Em). Note that these data are schematic, and were not obtained experimentally.

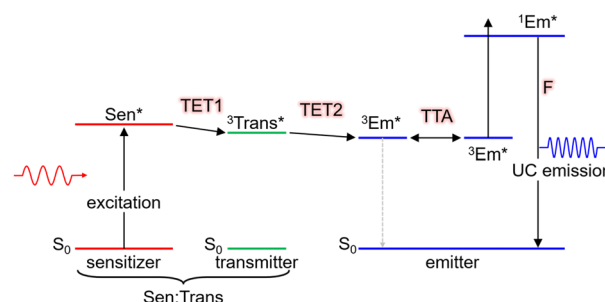by the phosphorescence lifetime (τ_{PL}) in the absence of the emitter:

$$k_{TET} = \frac{K_{SV}}{\tau_{PL}}. \qquad (7)$$

TET involves Dexter-type energy transfer, and its rate constant can be discussed using Marcus theory. Specifically, considering the sensitizer and emitter as the donor and acceptor of triplet energy, respectively, k_{TET} is described as follows:[21]

$$k_{TET} = \frac{|J|^2}{h}\sqrt{\frac{\pi}{\lambda k_B T}}\exp\left\{-\frac{\lambda}{4k_B T}\left(1 + \frac{\Delta G^\circ}{\lambda}\right)\right\}. \qquad (8)$$

In this equation, ΔG° represents the energy difference between the T_1 states of both molecules, $|J|$ is the electron coupling constant between the donor and acceptor, and λ signifies the reorganization energy.

Moreover, as illustrated in Scheme 2, when using nanoparticles as sensitizers, it is possible to efficiently transfer triplet energy to the emitter. In such cases, triplet energy transmitter ligands may be introduced onto the nanoparticle surface and additional free emitters may be added (Sen:Trans/Em). In this scenario, the overall TET comprises the first stage from the nanoparticle to the transmitter (TET1) and the second stage from the transmitter to the emitter (TET2). The overall Φ_{TET} is the product of Φ_{TET1} and Φ_{TET2}. TET1 can be evaluated

Scheme 2 Scheme of TTA-UC in the Sen:Trans/Em system (Sen = nanoparticles).

using transient absorption spectroscopy or phosphorescence lifetime measurements.

TTA efficiency

Although its definition may vary across different references, the term Φ_{TTA} is defined here as the probability of generating $^1\text{Em}^\star$ through the collision of $^3\text{Em}^\star$ molecules. Thus, Φ_{TTA} is expressed as the product of the spin statistical factor (f_{spin}) and the fraction (f_2) of the $^3\text{Em}^\star$ molecules generated by TET that are consumed in the deactivation processes, leading to TTA ($\Phi_{\text{TTA}} = 1/2f_{\text{spin}}f_2$). The value of f_2 is obtained by fitting the decay of the UC intensity based on kinetic considerations (Fig. 1, inset).[22–24] TTA involves reactions between triplet-sensitized $^3\text{Em}^\star$ molecules, and considering that it constitutes the latter part of the TTA-UC process, it is heavily dependent on the characteristics of the emitter molecules. As this review predominantly focuses on the triplet sensitization capability of the sensitizer in the first half of the TTA-UC process, detailed information about TTA may be referred to in other reports.[23,24]

Excitation intensity threshold

The TTA-UC process, being a bimolecular process, exhibits secondary behavior concerning the excitation light intensity (I_{ex}) in the low excitation intensity regime. However, efficient generation of $^3\text{Em}^\star$ occurs in the high excitation intensity regime, and TTA behaves in a pseudo-first-order manner. Therefore, plotting I_{UC} against I_{ex} shows a transition from secondary to primary behavior as I_{ex} increases (Fig. 3; in a log–log plot with the logarithm of I_{ex} on the horizontal axis and the logarithm of I_{UC} on the vertical axis, the slope of the plot gradually changes from 2 to 1). The excitation light intensity at this transition is referred to as the excitation intensity threshold (I_{th}). Thus, Φ_{UC} depends on the excitation light intensity, increasing with the increase in I_{ex} in the low excitation intensity regime, but reaching a constant value at excitation light intensities above I_{th}. I_{th} can be determined by drawing asymptotic lines with slopes of 1 and 2 on a log–log plot of I_{ex} vs. I_{UC} and finding the intersection, as shown in Fig. 3. Alternatively, I_{th}

can be evaluated using fitting functions based on kinetic interpretations.[25–27] For efficient energy conversion of low irradiance and incoherent light, such as the NIR light present in sunlight, a low value of I_{th} is desirable. Theoretically, I_{th} is expressed as:

$$I_{\text{th}} = (\varepsilon_{\text{Sen}}\Phi_{\text{TET}}8\pi D_{^3\text{Em}^*}a_0)^{-1}(\tau_{^3\text{Em}^*})^{-2}. \tag{9}$$

Here, ε_{Sen} is the molar absorption coefficient of the sensitizer under excitation light, $D_{^3\text{Em}^*}$ is the diffusion coefficient of $^3\text{Em}^\star$, a_0 is the distance between $^3\text{Em}^\star$ molecules in TTA, typically around 1 nm, and $\tau_{^3\text{Em}^*}$ is the lifetime of $^3\text{Em}^\star$.[28] Achieving lower thresholds for I_{th} is possible with larger values of these parameters.

General molecules for TTA-UC

Φ_{ISC} and Φ_{F} represent the unique properties of the sensitizer and emitter, respectively, whereas Φ_{TET} and Φ_{TTA} depend on the combination and concentration of sensitizer and emitter molecules. Therefore, to achieve more efficient TTA-UC, it is necessary to use sensitizers and emitters with a high Φ_{ISC} and Φ_{F} (~ 1). In many cases, sensitizers with a high Φ_{ISC}, large absorption cross-sections, and long excited-state lifetimes, such as phosphorescent materials (e.g., metalloporphyrins), are used, whereas emitters with high fluorescence quantum yields, such as 9,10-diphenylanthracene (DPA), perylene, and rubrene, are chosen. However, to absorb light in the desired NIR range, it is essential to extend the π-conjugated system of the organic sensitizer. In organic synthesis, this often requires complex reactions involving multiple steps, and such organic sensitizers face several challenges: (1) absorbing only specific wavelength ranges, limiting their application to a portion of the wide NIR spectrum in sunlight, and (2) photostability decreasing with the extension of the conjugated system.

In this review, the focus is not on organic sensitizers but on inorganic nanoparticles/crystals and nanoclusters composed of metals and semiconductors, which have recently garnered attention. The structures of the inorganic nano-sensitizers, emitters, and transmitter ligands introduced in this review are depicted in Fig. 4. The physical quantities related to TTA-UC with nanoparticles and nanoclusters presented in this review are summarized in Tables 1 and 2, respectively.

3. Inorganic nanoparticle sensitizers

Semiconductor nanoparticles (nanocrystals) with sizes ranging from a few to several tens of nanometers possess unique properties that differentiate them from organic sensitizers. These properties include (1) ease of synthesis, (2) tunability of electronic structure through size modulation, (3) a broad absorption spectrum spanning from visible to NIR light, (4) high photostability, and other characteristics not found in organic sensitizers. The recent award of the 2023 Nobel Prize in Chemistry for research on quantum dots underscores the significance of these semiconductor nanoparticles in the field of materials science.[29–32] In addition to their role as sensitizers,
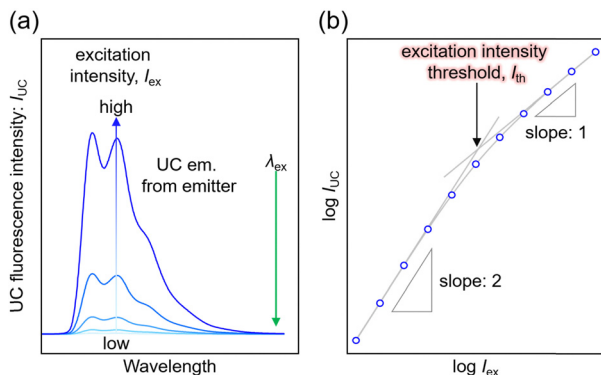

Fig. 3 (a) UC spectrum of the emitter as a function of excitation intensity and (b) log–log plot of UC intensity *versus* excitation intensity in a solution system consisting of sensitizer and emitter (Sen/Em). Note that these data were not obtained experimentally.
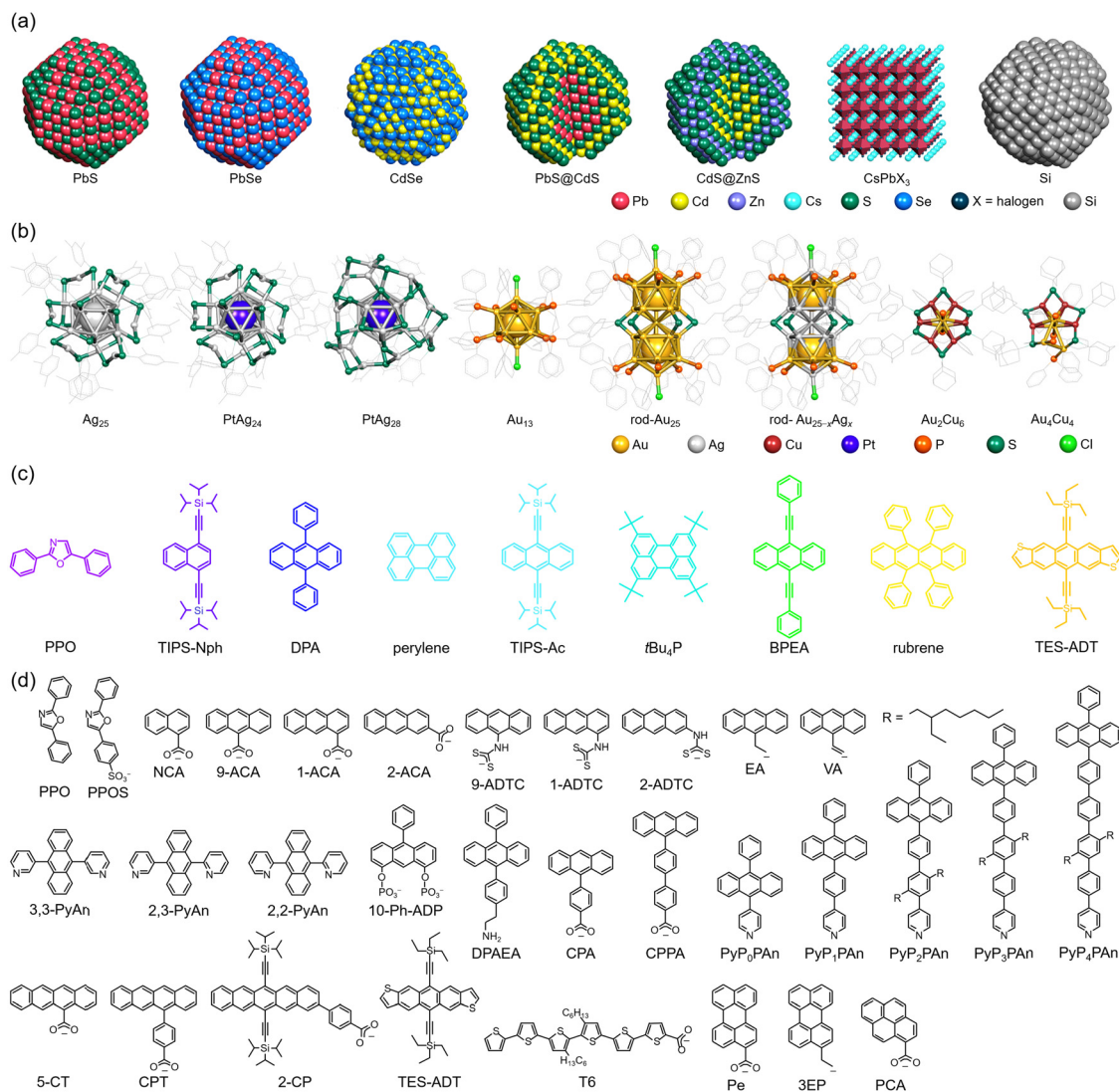
(a)

PbS   PbSe   CdSe   PbS@CdS   CdS@ZnS   CsPbX₃   Si

● Pb   ● Cd   ● Zn   ● Cs   ● S   ● Se   ● X = halogen   ● Si

(b)

Ag₂₅   PtAg₂₄   PtAg₂₈   Au₁₃   rod-Au₂₅   rod- Au₂₅₋ₓAgₓ   Au₂Cu₆   Au₄Cu₄

● Au   ● Ag   ● Cu   ● Pt   ● P   ● S   ● Cl

(c)

PPO   TIPS-Nph   DPA   perylene   TIPS-Ac   *t*Bu₄P   BPEA   rubrene   TES-ADT

(d)

PPO   PPOS   NCA   9-ACA   1-ACA   2-ACA   9-ADTC   1-ADTC   2-ADTC   EA   VA   R =

3,3-PyAn   2,3-PyAn   2,2-PyAn   10-Ph-ADP   DPAEA   CPA   CPPA   PyP₀PAn   PyP₁PAn   PyP₂PAn   PyP₃PAn   PyP₄PAn

5-CT   CPT   2-CP   TES-ADT   T6   Pe   3EP   PCA

Fig. 4 (a) Inorganic nanoparticle or nanocrystal sensitizers, (b) inorganic nanocluster sensitizers, (c) emitters/annihilator molecules, and (d) transmitter ligands. In (a), the protecting ligands on the surfaces of nanoparticles are omitted. In (b), counterions are omitted. In (c), the colors of the structures represent their emission colors.

these semiconductor nanoparticles have been studied for the TET from singlet fission-generated organic dye crystal layers to semiconductor nanoparticles.[33] In the following sections, we classify inorganic nanoparticles with sizes of a few nanometers based on their composition and shape, and we introduce the functions of these nanoparticles as triplet sensitizers and TTA-UC sensitizers, highlighting their roles in enhancing these processes.

Homogeneous nanoparticles

The initial application of inorganic nanoparticles in TTA-UC research was reported by Norris and Meinardi. However, in this study, inorganic nanoparticles are employed not as triplet sensitizers for fluorescent dyes, but as luminescent scavengers capable of absorbing UC fluorescence emitted from the solid-state TTA-UC and re-emitting it as long-wavelength light that can be further used in a TTA-UC process.[34] Subsequently, Tang

and colleagues initiated the use of inorganic nanoparticles as triplet sensitizers for fluorescent dyes.

Tang and Bardeen's group devised two strategies (A, B) to employ inorganic nanoparticles as sensitizers for TTA-UC.[35] The first strategy (A), as illustrated in Scheme 1, uses PbSe nanoparticle as sensitizers and rubrene as the emitter. In a TET process from 2.1 nm PbSe nanoparticle to rubrene, the T_1 state of rubrene is sensitized. Fig. 5(a) and (b) depicts the UC emission and excitation intensity dependence when a 980 nm CW laser is irradiated onto the PbSe/rubrene solution. Upon NIR irradiation, distinct yellow UC emission from rubrene is observed, with a quantum yield (Φ_{UC}) of 0.005% ($\Phi'_{UC} = 0.01\%$). Because TET is a Dexter-type energy transfer, its efficiency should depend on the overlap of the wave functions for the sensitizer and emitter molecules (eqn (8)). Consequently, the UC emission of rubrene was observed using PbS nanoparticles with a smaller Bohr radius as sensitizers. As anticipated, the UC intensity in the PbS/rubrene

Table 1 Summary of TTA-UC quantities in inorganic nanoparticle systems

Sensitizer[a]	Transmitter	Emitter	λ_{ex}/nm	k_{TET}/s^{-1} [b] (Φ_{TET}%)	ΔE_{AS}/eV	Φ_{UC}%[c] [Φ_{UCg}%]	I_{th}/mW cm^{-2}	Ref.
PbSe (2.1 nm)	—	Rubrene	800	—	0.92	0.005	$\sim 6 \times 10^4$	35
CdSe (2.7 nm)	9-ACA	DPA	532	TET1: 1.5×10^7	0.54	4.5	$\sim 1 \times 10^4$	35,38
CdSe (2.4 nm)	9-ACA	DPA	488	TET1: 3.8×10^7	0.33	6.0	—	39
	1-ACA	DPA	488	TET1: 0.077×10^7	0.33	1.5	—	39
	2-ACA	DPA	488	TET1: 0.063×10^7	0.33	0.6	—	39
	1-ADTC	DPA	532	TET1: 0.075×10^7	0.54	1.5	—	39
	2-ADTC	DPA	532	TET1: 0.063×10^7	0.54	0.5	—	39
	9-ADTC	DPA	488	TET1: 2.7×10^7	0.33	0.05	—	39
CdSe (3.3 nm)	Pe	tBu$_4$P	532	TET1: 3.7×10^8 (47.2)	0.26	3.5	~ 100	40
CdSe (4.2 nm)	Pe	tBu$_4$P	532	TET1: 3.4×10^8 (11.4)	0.26	0.28	~ 2000	40
CdTe (3.4 nm)	Pe	tBu$_4$P	532	TET1: 4.0×10^8 (25.6)	0.26	1.0	~ 500	40
CdTe (3.7 nm)	Pe	tBu$_4$P	532	TET1: 1.2×10^8 (7.51)	0.26	0.09	$\sim 1.2 \times 10^4$	40
CdSe (2.6 nm)	9-ACA	DPA	532	TET1: $\sim 2.7 \times 10^6$ (30.5)	0.54	7.2	—	41
	CPA	DPA	532	TET1: $\sim 6.6 \times 10^5$ (7.8)	0.54	2.0	—	41
	CPPA	DPA	532	TET1: $\sim 8.9 \times 10^4$ (0.85)	0.54	0.2	—	41
CdSe (2.4 nm)	2,3-PyAn	DPA	532	TET1: 1.28×10^9 (42.0) TET2: (61.4)	0.54	6.1	146.8	43
	3,3-PyAn	DPA	532	TET1: 9.62×10^8 (38.1) TET2: (45.4)	0.54	4.1	—	43
	2,2-PyAn	DPA	532	TET1: 1.25×10^9 (23.1) TET2: (23.1)	0.54	1.3	—	43
CdSe (2.4 nm)	10-Ph-ADP	DPA	488	TET1: 1.22×10^{11} (86.4)	0.34	8.5	163	44
	9-ACA	DPA	488	TET1: 5.98×10^{10} (84.7)	0.34	6.4	492	44
PbS (2.9 nm)	CPT	Rubrene	808	—	0.68	0.85		45
	—	Rubrene	808	—	0.68	0.011		45
PbSe (2.5 nm)	CPT	Rubrene	808	—	0.68	1.1		45
	—	Rubrene	808	—	0.68	0.10		45
PbS (2.7 nm)	5-CT	Rubrene	781	TET1: 2.56×10^9 (69.5)	0.63	5.9	5.34×10^4	46
PbS (1.27 eV)[d]	TES-ADT	TES-ADT	1064	TET1: 2×10^8 (8.8)	0.86	0.047	4.3×10^4	51
PbS@CdS (2.7@0.24 nm)	5-CT	Rubrene	808	—	0.68	4.2	3.2	54
PbS (2.7 nm)	5-CT	Rubrene	785	TET1: 5.91×10^9 (60.3)	0.63	1.8		55
PbS@CdS (2.7@0.25 nm)	5-CT	Rubrene	785	TET1: 1.03×10^9 (71.8)	0.63	2.5		55
PbS (3.3 nm)	—	Rubrene	785	—	0.63	0.0002	—	56
PbS@ZnS (3.22@0.004 nm)	—	Rubrene	785	—	0.63	0.14	—	56
PbS@CdS (3.11@0.060 nm)	—	Rubrene	785	—	0.63	0.065	—	56
CdS@ZnS (3.6@1.2 nm)	PPO	PPO	405	TET1: 14.9×10^9 (88)	0.43	2.6	~ 2000	57
CsPb(Br/I)$_3$ (7.5 nm)	DPAEA	DPA	532	TET1: (38)	0.53	0.65	25	58
CsPb(Cl/Br)$_3$ (9.4 nm)	NCA	PPO	405	TET1: (32)	0.43	2.6	4700	59
CsPbBr$_3$ (2.42 eV)[e]	PPOS	TIPS-Nph	515	—	0.90	0.007	1600	60
Ce–CsPbBr$_3$ ($\sim$6 nm)	PCA	DPA	450	TET1: 3.6×10^8 (60)	0.32	2.4		61
Si (3.1 nm)	9EA	DPA	488	—	0.33	8.59	—	63
Si (3.4 nm)	3EP	tBu$_4$P	532	TET1: 2.4×10^5 TET2: 1.4×10^4	0.28	0.75	< 25	64
			640		0.67	0.21	< 80	64
			730		0.91	—	—	64
Si (3.1 nm)	9EA	DPA	488	TET1: 6.57×10^7 (48)	0.38	3.5	950	65
			532		0.59		2000	65
			640		0.98	0.05		65
Si (3.1 nm)	9VA	DPA	485	ISC: $3 \times 10^{8 f}$	0.33	1.8	1500	66
		tBu$_4$P	532		0.28	4.0 [8.6]	500	66

[a] The values in bracket represent diameter of nanoparticles. For core–shell nanoparticles, the core diameter and shell thickness are separated by "@". [b] In this column, the rate constants k_{TET} and Φ_{TET} (values in ()) in TET1 or TET2 are indicated. [c] The internal UC efficiency (Φ_{UCg}) is described in []. Theoretical maximum of both Φ_{UC} and Φ_{UCg} are 50%. [d] Absorption energy. The diameter of the nanoparticles was not described in the literature. [e] Photoluminescence energy. The diameter of the nanoparticles was not described in the literature. [f] The intersystem-crossing rate that converts a spin-singlet state localized on the Si nanoparticle to a spin-triplet state that spatially extends across the Si:9VA interface.

system was approximately 3.5 to 3.8 times weaker than that in the PbSe/rubrene system. These experiments demonstrated that the Bohr radius of the nanoparticles is one key factor influencing the efficiency of TTA-UC using semiconductor nanoparticles as sensitizers.[35] Additionally, experimental results revealed that the value of K_{SV} between PbSe nanoparticles and rubrene is < 200 M^{-1}. This implies that the TET in PbSe/rubrene is in the normal region according to Marcus theory.[36]

In the alternative strategy (B), as depicted in Scheme 2, the formed excited triplet state moves from a sensitizer to a transmitter ligand through TET1, and subsequently, through TET2 from the transmitter ligand to the emitter, enhancing the ³Em*. Tang and colleagues synthesized nano-complex sensitizers (CdSe:9-ACA) by replacing the octadecylphosphonic acid ligands (ODPA) on the surfaces of 3.3 nm CdSe nanoparticles with 9-anthracene carboxylic acid (9-ACA). These sensitizers were then combined with the emitter, DPA. In this approach, the triplet energy generated in CdSe nanoparticles efficiently forms the T$_1$ state of DPA, mediated by 9-ACA as the triplet energy transmitter. Notably, in the simple mixed system of

Table 2 Summary of TTA-UC quantities in inorganic nanocluster systems

Sensitizer	Emitter	λ_{ex}/nm	k_{TET}/s$^{-1\,a}$ [K_{SV}/M^{-1} s^{-1}] (Φ_{TET}%)	ΔE_{AS}/eV	Φ_{UC}%^{b} [Φ_{UCg}%]	I_{th}/mW cm^{-2}	Ref.
Ag$_{25}$	Perylene	640	1.51×10^7 [15.7] (14)	0.68	8.1×10^{-5} [4.1×10^{-4}]	—	74
	TIPS-Ac	640	1.53×10^7 [15.9] (14)	0.68	2.9×10^{-4} [1.7×10^{-3}]	—	74
PtAg$_{24}$	Perylene	640	1.55×10^8 [290] (76)	0.67	1.9 [5.4]	3800	74
		785		1.04	1.1 [3.1]	$>1.4 \times 10^4$	74
	TIPS-Ac	640	1.95×10^8 [366] (83)	0.67	0.87 [2.8]	120	74
		780		1.03	1.2 [3.9]	1100	74
PtAg$_{28}$	DPA	532	2.13×10^8 [1400] (91)	0.52	6.1 [12.2]	0.81	79
Au$_{13}$	Perylene	640	9.08×10^7 [237.5]	0.69	—	—	87,88
rod-Au$_{25}$	BPEA	640	4.6×10^6 [15.5] (24.9)	0.50	0.665 [1.9]^a	—	93
	Rubrene	785	9.5×10^7 [320.1] (75)	0.52	0.057 [0.13]^a	—	93
rod-Au$_{25-x}$Ag$_x$	Perylene	640	1.5×10^8 [1200] (83)	0.69	4.7 [12.6]^a	6.8	107
Au$_2$Cu$_6$	Perylene	532	1.91×10^7 [93.9] (32)	0.30	0.18 [0.30]^a	—	110
	DPA	532	2.32×10^5 [1.14] (2.2)	0.52	—	—	110
		640		0.95	0.18 [0.36]^a	>5000	112
Au$_4$Cu$_4$	Perylene	640	1.98×10^8 [1570] (98)	0.70	1.6 [3.2]^a	1200	112
	DPA	532	1.32×10^7 [105] (81)	0.52	6.4 [13.7]^a	2.5	112
		640		0.95	6.6 [14.0]^a	26	112

^{a} In this column, the rate constants k_{TET}, K_{SV} (values in [ ]), and Φ_{TET} (values in ( )) are listed. ^{b} The internal UC efficiency (Φ_{UCg}) is described in [ ]. Theoretical maximum of both Φ_{UC} and Φ_{UCg} are 50%.
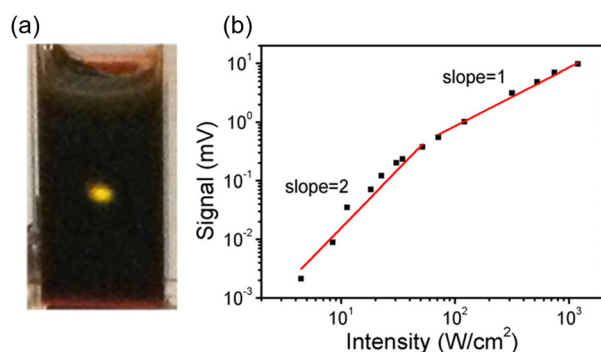

Fig. 5 (a) UC fluorescence from PbSe/rubrene excited at 980 nm CW laser and (b) excitation intensity dependency of UC intensity form PbSe/rubrene. Reproduced from ref. 35 with permission from American Chemical Society, Copyright 2015.
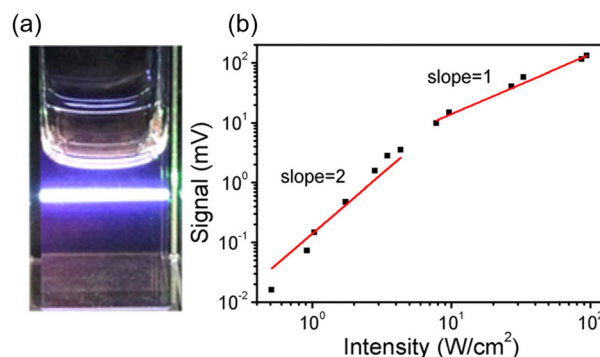

Fig. 6 (a) UC fluorescence from CdSe:9-ACA/DPA excited at 532 nm CW laser and (b) excitation intensity dependency of UC intensity form CdSe:9-ACA/DPA. Reproduced from ref. 35 with permission from American Chemical Society, Copyright 2015.

CdSe nanoparticles and DPA (CdSe/DPA; Scheme 2), no blue UC emission was observed from DPA under green excitation light at 532 nm, possibly owing to the small Bohr radius of CdSe nanoparticles (4–5 nm). For the CdSe:9-ACA/DPA system, blue UC emission was observed from green excitation light (532 nm) with $\Phi_{UC} = 4.5\%$ ($\Phi'_{UC} = 9\%$) (Fig. 6(a) and (b)).[35] Subsequent detailed experiments by the same group on the CdSe:9-ACA/DPA system using Strategy B revealed that the UC efficiency is higher when there are more 9-ACA transmitters on the surfaces of CdSe nanoparticles. Additionally, they found a direct correlation between Φ'_{UC} and the nanoparticle's photoluminescence quantum yield Φ_{PL} and an indirect correlation with nanoparticle size.[37] Then, they performed time-resolved photoluminescence spectroscopy and determined that the energy transfer rate constant (k_{TET1}) from CdSe nanoparticles to 9-ACA transmitters is 1.5×10^7 s^{-1}.[38]

In addition to introducing carboxylic acid at the 9-position of anthracene, carboxylic acid can also be introduced at the 1- and 2-positions. Furthermore, not only carboxylic acid derivatives of

anthracene but also three isomers of dithiocarbamate (ADTC) derivatives of anthracene (1-ADTC, 2-ADTC, 9-ADTC) can be used as transmitters in TTA-UC. For TTA-UC in solution systems (CdSe:Trans/DPA, Trans = 1-ACA, 2-ACA, 9-ACA and 1-ADTC, 2-ADTC, 9-ADTC) consisting of CdSe nanoparticles and complexes with these ACA or ADTC transmitters along with DPA, the highest efficiency was obtained using 9-ACA, with $\Phi_{UC} = 6\%$ ($\Phi'_{UC} = 12\%$), and the lowest efficiency was observed using 9-ADTC, with $\Phi_{UC} = 0.05\%$ ($\Phi'_{UC} = 0.1\%$). Using 1-ACA and 1-ADTC resulted in a Φ_{UC} of 1.5% ($\Phi'_{UC} = 3\%$), and using 2-ACA and 2-ADTC yielded a Φ_{UC} of 0.5% ($\Phi'_{UC} = 1\%$). This suggests that in TET based on Dexter-type energy transfer, the overlap of orbitals between the triplet energy donor and acceptor is crucial (eqn (7)), and the orientation of the transmitter with respect to the nanoparticle sensitively affects the efficiency of TET1.[39]

The group led by Yanai, Kimizuka, Teranishi, and Sakamoto systematically evaluated TET1 and TTA-UC in systems where perylene-3-carboxylic acid (Pe) was complexed as a transmitter ligand on the surfaces of CdX nanoparticles (X = Se, Te), namely

CdX:Pe, and in CdX:Pe/tBu_4P systems (tBu_4P = 2,5,8,11-tetra-*tert*-butylperylene). They systematically varied the chalcogen X, nanoparticle size, and number of Pe ligands. The efficiency of TET1 depended on the triplet exciton energy of the nanoparticles, with smaller nanoparticles (larger bandgap) showing improved TET1 efficiency. However, reducing the size led to a decrease in surface area, suppressing the coordination number of Pe. They emphasized the importance of optimizing this balance to achieve high TET1 efficiency.[40]

Detailed research has been conducted on the kinetics of TET1 between semiconductor nanoparticles and transmitter ligands. Generally, the rate constant for Dexter-type energy transfer in TET is exponentially reduced with the distance (d) between the triplet donor and acceptor, as expressed in the following equation:[41]

$$k_{TET} = k_0 \exp(-\beta d) \qquad (10)$$

Here, β is the attenuation factor, and k_0 is the rate constant when the donor–acceptor distance is 0. Tang and colleagues used three transmitters (9-ACA, CPA (4-(anthracene-9-yl)benzoic acid), and CPPA (4′-(9-anthracenyl)[1,1′-biphenyl]-4-carboxylic acid)), in which they controlled the distance (number of phenylene units) between the anthracene moiety and the carboxylic acid anchor. They coordinated these transmitters to the surfaces of CdSe nanoparticles and evaluated the distance dependence of the TET1 rate constant from the CdSe nanoparticle surface to anthracene. The TET1 rate constant exponentially decayed with the distance d, and the attenuation factor β was estimated to be 0.43 ± 0.07 Å^{-1} (Fig. 7(a)).[41] In mixtures of nanoparticle sensitizers with these transmitter ligands and DPA emitters, there was a correlation between the TET1 rate constant and Φ_{UC}. In the optimal system, green excitation light (532 nm) was upconverted to blue light, reaching Φ_{UC} = 7.2% (Φ'_{UC} = 14.3%).[41]

Furthermore, a transmitter, namely PyPxPAn (x = 0–4; 4-(10-phenylanthracen-9-yl)pyridine (PyP0PAn), 4-(4-(10-phenylanthr-acen-9-yl)phenyl)pyridine (PyP1PAn), 4-(2,5-bis(2-ethylhexyl)-4′-(10-phenylanthracen-9-yl)-[1,1′-biphenyl]-4-yl)pyridine (PyP2PAn), 4-(2′,5′-bis(2-ethylhexyl)-4″-(10-phenylanthracen-9-yl)-[1,1′:4′,1″-ter-phenyl]-4-yl)pyridine (PyP3PAn), 4-(2′,5′-bis(2-ethylhexyl)-4‴-(10-phenylanthracen-9-yl)-[1,1′:4′,1″:4″,1‴-quaterphenyl]-4yl)pyridine (PyP4PAn)), was developed by the same group, where the distance between 10-phenylanthracene (PAn) and pyridine (Py) was controlled by the number of phenylene units x (Fig. 7(b)). For the CdSe:PyPxPAn/DPA system, where CdSe nanoparticles were complexed with PyPxPAn and mixed with DPA, the Φ_{UC} decreased as the number of phenylene units x increased from 0 to 2 (Φ_{UC} = 5.8% (x = 0), 2.26% (x = 1), 0.142% (x = 2) (Φ'_{UC} = 11.6% (x = 0), 4.51% (x = 1), 0.284% (x = 2)). However, an increasing trend in Φ_{UC} was observed for x = 3 and 4 (Φ_{UC} = 0.234% (x = 3), 0.206% (x = 4) (Φ'_{UC} = 0.468% (x = 3), 0.413% (x = 4)). Up to x = 2, Dexter-type TET1 from CdSe to PAn occurred with the attenuation factor β = 0.724 Å^{-1}. However, reaching x = 3 and 4, a transition from exciton tunneling to hopping effects occurred, leading to TET1 that did not depend on distances, beyond the conventional Dexter distance (~1 nm).[42]
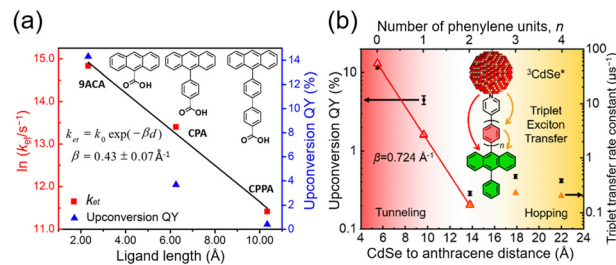

Fig. 7 Distance dependence of the TET rate constant and UC efficiency in (a) CdSe:X/DPA (X = 9-ACA, CPPA, CP4A) and (b) CdSe:PyPxPAn/DPA (x = 0–4) systems. Reproduced from ref. 41 with permission from Journal of American Chemical Society, Copyright 2016 and ref. 42 with permission from American Chemical Society, Copyright 2020.

Additionally, molecules capable of bidentate coordination have been employed as transmitters. For instance, isomers of bis(pyridine)anthracene, such as 2-(10-(pyridin-3-yl)anthracen-9-yl)pyridine (2,3-PyAn), 9,10-di(pyridin-3-yl)anthracene (3,3-PyAn), and 9,10-di(pyridin-2-yl)anthracene (2,2-PyAn), were complexed with CdSe nanoparticles and evaluated in solution systems with DPA. It was revealed that (1) TET1 from CdSe to the transmitter is correlated with UC efficiency, and (2) there is a tendency for Φ'_{UC} to be higher in the order of 2,2-PyAn < 3,3-PyAn < 2,3-PyAn.[43] Furthermore, phosphoric acid-based transmitters, such as 10-phenylanthracene-1,8-diyl bis(dihydrogen phosphate) (10-Ph-ADP) with phosphoric acid anchors introduced at the 1,8-positions of anthracene, have been developed. For the system where CdSe and 10-Ph-ADP are complexed (CdSe:10-Ph-ADP) and mixed with DPA in solution, a Φ_{UC} of 8.5% (Φ'_{UC} = 17%) was recorded, demonstrating higher performance compared with CdSe:9-ACA/DPA (Φ_{UC} = 6.5%; Φ'_{UC} = 13%). Transient absorption spectroscopy revealed that the 10-Ph-ADP transmitter has a lifetime characteristic of the T_1 state that is 3.4 times longer than that of 9-ACA.[44]

Transmitters with extended conjugation in the acene series have been developed to lower the T_1 energy of the transmitter, achieving an efficient energy cascade. Tang and colleagues synthesized PbX:CPT (X = S or Se) nanostructures, where tetracene-based 4-(tetracene-5-yl)benzoic acid (CPT) transmitters with slightly higher T_1 energy than rubrene were
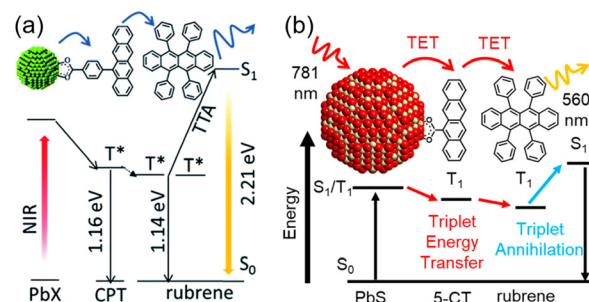

Fig. 8 (a) TTA-UC scheme for the PbX:CPT/rubrene system. Reproduced from ref. 45 with permission from Royal Society of Chemistry, Copyright 2016. (b) TTA-UC scheme for the PbS:5-CT/rubrene system. Reproduced from ref. 46 with permission from American Chemical Society, Copyright 2019.
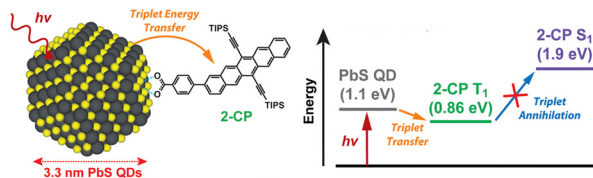
Fig. 9 PbS:2-CP and its TET scheme. Reproduced from ref. 47 with permission from American Chemical Society, Copyright 2018.

Fig. 10 TTA-UC scheme for PbS:TES-ADT/TES-ADT. Reproduced from ref. 51 with permission from Royal Society of Chemistry, Copyright 2019.

complexed on the surfaces of CdX (X = S or Se) nanoparticles (Fig. 8(a)). They successfully achieved an efficient TET cascade from these PbX:CPT sensitizers to rubrene, converting NIR excitation light (808 nm) into yellow emission with a Φ_{UC} of ~1% (Φ'_{UC} of ~2%).[45] Additionally, using highly pure lead and thiourea precursors, PbS nanoparticles were synthesized and complexed with 5-carboxylic acid tetracene (5-CT) transmitters, resulting in the sensitizer PbS:5-CT. In a mixture system of PbS:5-CT/rubrene, this sensitizer efficiently upconverted 781 nm NIR excitation light to 560 nm yellow emission with $\Phi_{UC} = 5.9\%$ ($\Phi'_{UC} = 11.8\%$) (Fig. 8(b)). The high UC performance is attributed to (1) improved crystallinity leading to longer lifetimes of PbS excitons and (2) the long lifetime of the T_1 state in the 5-CT transmitter.[46]

Among acene-based transmitters, the pentacene derivative 4-(6,13-bis(2-(triisopropylsilyl)ethynyl)pentacen-2-yl)benzoic acid (2-CP) has the longest conjugation (Fig. 9). The sensitizer PbS:2-CP, using PbS nanoparticles with a diameter of 3.3 nm, were complexed with 2-CP, and the energy transfer from PbS to the transmitter was studied in detail. Transient absorption spectroscopy and density functional theory (DFT) calculations revealed that PbS:2-CP forms a charge carrier intermediate localized on the nanoparticle surface within 40 ps of photo-excitation and subsequently forms the T_1 state of 2-CP over 100 ns.[47] The 2-CP transmitter and similar compounds have been used as molecules that achieve efficient singlet fission in several instances.[48,49]

Evangelista, Egap, and Lian's group evaluated the performance of TET1 in a complex (CdSe:T6) where oligothiophene carboxylic derivative 3‴,4‴-dihexyl-[2,2′:5′,2″:5″,2‴:5‴,2⁗:5⁗,2⁗′-sexithiophene]-5-carboxylic acid (T6) was coordinated as a transmitter on the surfaces of oleic acid-protected CdSe nanoparticles. According to transient absorption spectroscopy results, in a 1:1 complex of CdSe and T6, k_{TET1} from CdSe to T6 was determined to be 0.077 ns^{-1}. Unlike previously reported acene-based transmitters, thiophene-based transmitters offer high stability and flexible molecular design, supporting further progress in this field.[50]

Designing an energy cascade for the entire TTA-UC system through the transmitter ligand is crucial for achieving efficient TTA-UC. However, multi-step energy transfer can lead to energy losses. Rao and colleagues addressed this challenge by finding a way to minimize energy losses (Fig. 10). They demonstrated that 1) 5,11-bis(triethylsilylethynyl)anthradithiophene (TES-ADT) binds to PbS nanoparticles and rapidly extracts triplet energy from the excited state of PbS ($k_{TET1} \sim 2 \times 10^8$ s^{-1}), and 2) the triplet-sensitized ^{3}(TES-ADT)* also acts as an annihilator in TTA-UC. By leveraging these behaviors, they successfully
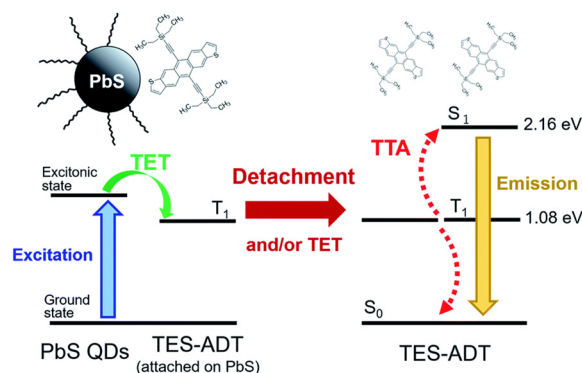
upconverted 1064 nm NIR excitation light to 610 nm visible light in the PbS:TES-ADT/TES-ADT system ($\Delta E_{AS} = 0.86$ eV, $\Phi_{UC} = 0.047\%$, $I_{th} = 43$ W cm^{-2}). The use of the TES-ADT, serving as both a transmitter and emitter, helps achieve relatively high Φ_{TET} (8.8 ± 0.8% in a 50 mM TES-ADT solution), even with a relatively small TET driving force between PbS sensitizer and TES-ADT, enabling high-efficiency TET that was not possible with conventional annihilators.[51]

Deployment of nanoparticle sensitizers and emitters into solid-state devices has also been achieved. Baldo and colleagues developed a solid-state device by dispersing a monolayer of CdS nanoparticles on a glass substrate and casting a film of rubrene crystal containing red-emitting dibenzotetraphenylperiflanthene (DBP) on top. In this case, the rubrene crystal acts as both the annihilator for triplet excitons and the diffusion field for singlet excitons. UC occurs through energy transfer from singlet excitons in the rubrene crystal to DBP. Using three CdS nanoparticles of different sizes to control the absorption wavelength, the estimated Φ_{UC} and I_{th} ranged from 1.2% to 0.21% and 12 to 26 mW cm^{-2} for 808 nm excitation, respectively. This study further demonstrated the conversion of NIR excitation light with a wavelength exceeding 1 μm (using an absorption intensity less than one sun) to red emission at 612 nm.[52] Very recently, solid-state UC materials combining PbS nanoparticles as sensitizers, TES-ADT as transmitter/annihilator, and DBP dye have also been developed.[53]

Core–shell nanoparticles

The main advantage of nanoparticles is the modulation of their electronic structure with small changes in their size and structure. Core–shell nanoparticles with distinct compositions in the interior and on the surface have several beneficial properties in the context of TTA-UC.

As an example, we describe the TTA-UC characteristics of PbS@CdS core–shell nanoparticles in a rubrene solution (PdS@CdS/rubrene), as reported by Tang and coworkers.[54] In such systems, increasing the thickness of the CdS shell while maintaining the nanoparticle size leads to an increase in Φ'_{UC} (Fig. 11(a)). This phenomenon is attributed to the CdS shell suppressing nonradiative recombination by passivating trap
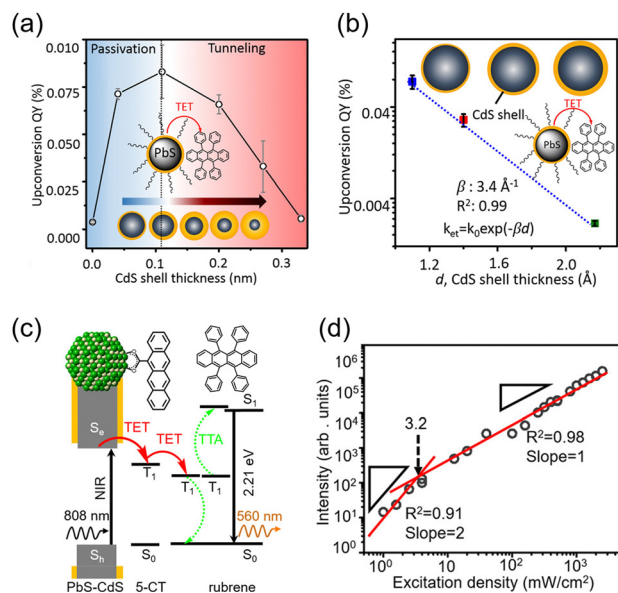
Fig. 11 (a) Φ_{UC} in the PbS@CdS/rubrene system when the particle size was constant and the CdS shell thickness was changed. (b) Φ_{UC} in the PbS@CdS/rubrene system when the core PbS size was constant and the CdS shell thickness was changed. (c) TTA-UC mechanism in the PbS@CdS:5-CT/rubrene system. (d) Log–log plot of UC intensity *versus* excitation intensity in the PbS@CdS:5-CT/rubrene system. Reproduced from ref. 54 with permission from American Chemical Society, Copyright 2016.

states and the enhanced efficiency of TET due to the increase in bandgap (E_g) with decreasing core size. Further thickening of the shell results in a decrease in Φ'_{UC}. In these particles, the CdS shell functions as an insulating layer ($\beta = 3.4$ Å^{-1}, eqn (10)), inhibiting the wavefunction overlap between the PbS core and rubrene, thus explaining this behavior (Fig. 11(b)). For the PdS@CdS with the highest Φ_{UC}, a solution system containing tetracene-based 5-CT transmitter and rubrene (PdS@CdS:5-CP/rubrene; Fig. 11(c)) resulted in a Φ_{UC} of 4.2% ($\Phi'_{UC} = 8.4\%$). This Φ_{UC} is approximately 37 times higher compared with the solution system without a transmitter (PdS@CdS/rubrene). Additionally, PdS@CdS:5-CP/rubrene exhibits an extremely low I_{th} of 3.2 mW cm^{-2} (Fig. 11(d)).[54] Moreover, in systems where PbS nanoparticles are complexed with a tetracene-based transmitter (5-CT) (PbS:5-CT/rubrene), covering the PbS core with a CdS shell (PbS@CdS:5-CT/rubrene) suppresses hole transfer from the PbS core to 5-CT, enhancing Φ_{TET} and Φ_{UC}.[55] Additionally, Zn and Cd adsorption on the surfaces of PbS nanoparticles induces defect levels, enhancing TTA-UC efficiency by up to 700-fold and 325-fold, respectively, compared with pristine PbS.[56] 2,5-diphenyloxazole (PPO) possesses properties of both an emitter and a transmitter. In the solution system using CdS@ZnS core–shell nanoparticles and PPO (CdS@ZnS:PPO/PPO), a maximum Φ_{UC} of 2.6% ($\Phi'_{UC} = 5.2\%$) has been reported, achieving UC of 405 nm blue excitation light to 355 nm UV light.[57]

Perovskite nanocrystals

Perovskite-type CsPbX$_3$ (X = halogen) nanocrystals are capable of altering excitonic properties by changing the halogen type.

Owing to their small exciton binding energy and high absorption cross-section, these nanocrystals are suitable for light-harvesting in solar cells.

Yanai and Kimizuka *et al.* developed a sensitizer (CsPbX$_3$:DPAEA) by partially replacing the oleylamine surface-protecting ligands of CsPbX$_3$, (X = Br/I) nanocrystals with an amine derivative of DPA, 4-(10-phenyl-9-anthracenyl)benzeenethanamine (referred to as DPAEA in this manuscript) (Fig. 12(a)). The evaluation of the photoluminescence lifetimes for the CsPb(Br/I)$_3$ and CsPb(Br/I)$_3$:DPAEA sensitizer indicated a Φ_{TET1} of 0.38 from CsPbX$_3$ to the DPAEA transmitter. In the solution system composed of CsPb(Br/I)$_3$:DPAEA and DPA emitter (CsPb(Br/I)$_3$:DPAEA/DPA), UC from 532 nm to 434 nm was observed, with $\Phi_{UC} = 0.65\%$ ($\Phi'_{UC} = 1.3\%$) and $I_{th} = 25$ mW cm^{-2} (Fig. 12(b)–(d)).[58] Subsequently, the same group achieved TTA-UC from visible light to UV light in another system. They successfully developed a sensitizer (CsPbX$_3$:NCA) by coordinating a naphthalene-based 1-naphthoic acid (NCA) transmitter on the surfaces of CsPbX$_3$ nanocrystals with different halogens (X = Cl/Br). The Φ_{TET1} from CsPb(Cl/Br)$_3$ to NCA was estimated to be 0.32, and by mixing CsPb(Cl/Br)$_3$:NCA with PPO emitter, they achieved the UC of 445 nm visible excitation light to 363 nm UV light ($\Delta E_{AS} = 0.63$ eV, $\Phi_{UC} = 2.6\%$ ($\Phi'_{UC} = 5.2\%$), $I_{th} = 4.7$ W cm^{-2}).[59] Furthermore, the group introduced 4-(2-phenyloxazol-5-yl)benzenesulfonate (PPOS) as a transmitter ligand on the surfaces of CsPbBr$_3$ nanocrystals and combined it with a naphthalene derivative emitter 1,4-bis((triisopropyl-silyl)ethynyl)naphthalene (TIPS-Nph). This combination achieved TTA-UC from 515 nm green excitation light to 375 nm UV light ($\Delta E_{AS} = 0.90$ eV, $\Phi_{UC} = 0.007\%$ ($\Phi'_{UC} = 0.014\%$), $I_{ex} = 16$ W cm^{-2}).[60]

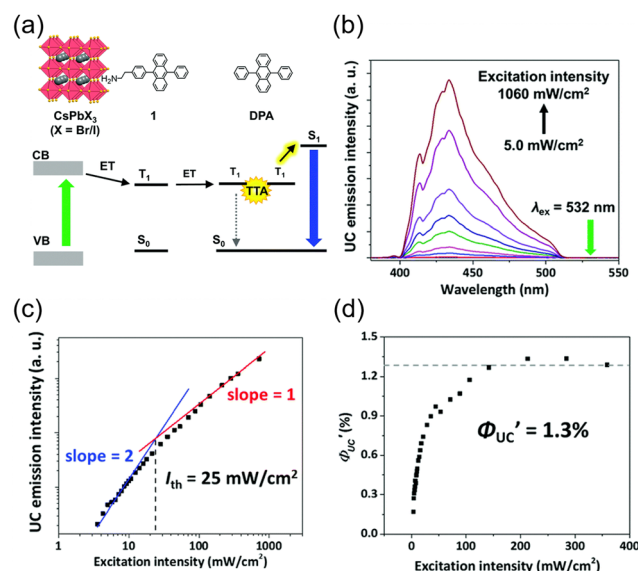**Fig. 12** (a) Scheme of TTA-UC for CsPb(Br/I)$_3$:DPAEA/DPA. (b) UC spectra of free DPA measured at various excitation intensities using a 532 nm laser. (c) Excitation intensity dependence of UC intensity at 430 nm for CsPb(Br/I)$_3$:DPAEA/DPA. (d) Excitation intensity dependence of Φ'_{UC}. Reproduced from ref. 58 with permission from Royal Society of Chemistry, Copyright 2017.

Xu and coworkers developed a sensitizer that is a complex of $CsPbBr_3$ nanocrystals and 1-pyrenecarboxylic acid (PCA) as transmitter. This composite recorded a Φ_{UC} of 0.85% when mixed with DPA, while Ce–$CsPbBr_3$, in which $CsPbBr_3$ nanocrystals were doped with cerium (Ce), was found to improve the Φ_{UC} to 2.40%. Interestingly, the efficiency of TET1 varies with the amount of Ce doping, indicating that doping can tune the electronic structure for suitable TTA-UC.[61]

Metal-free nanoparticles

In the aforementioned inorganic nanoparticle sensitizers, heavy metal elements, such as Cd and Pb, are used. However, such inorganic nanoparticles exhibit weak electronic coupling with organic transmitter molecules on their surfaces. As a result, the carrier wave functions excited in the nanoparticles tend to be localized either within the internal regions or on the surfaces of the nanoparticles.
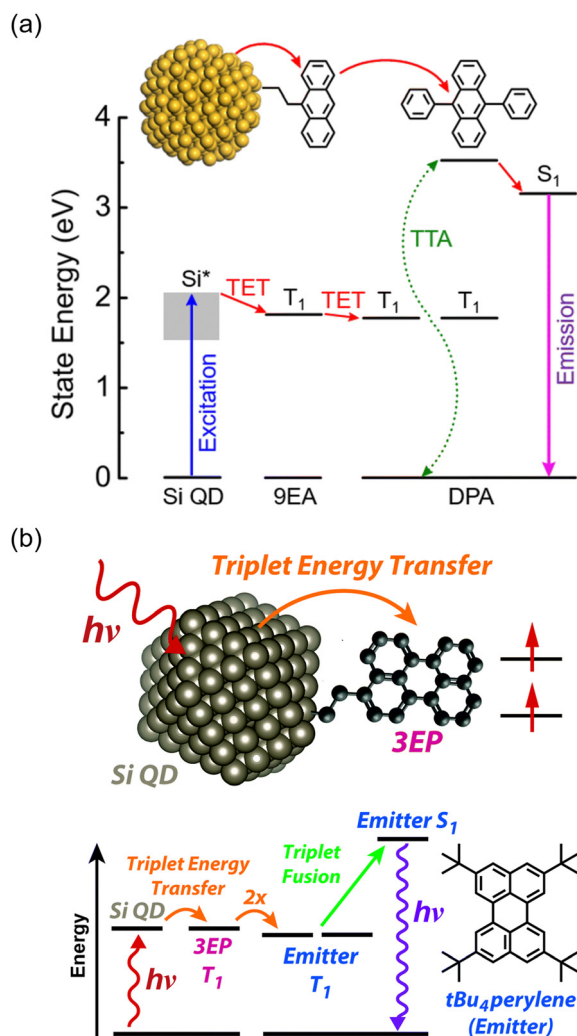
In recent studies by Tang and colleagues, nanoparticles made of silicon, in addition to semiconductor nanoparticles, have been employed as sensitizers. Silicon is an abundant element on Earth, and because of its low toxicity, it has gained attention as a clean material. Silicon nanoparticles are expected to have a very small gap (~ 10 meV) between bright exciton states and dark triplet states, allowing for efficient triplet generation.[62]

Tang and colleagues synthesized Si:9EA or Si:3EP nanoparticle complexes by reacting 9-vinylanthracene or 3-vinylperylene with silicon nanoparticles protected by alkane, resulting in the binding of 9-ethylanthracene (9EA) or 3-ethylperylen (3EP) to the surfaces of silicon nanoparticles with a diameter of ~ 3 nm (Fig. 13).[63,64] In the solution system composed of Si:9EA and DPA (Si:9EA/DPA), UC from 488–640 nm excitation light to 425 nm fluorescence was achieved with a maximum Φ_{UC} of 3.5% $(\Phi'_{UC} = 7\%)$.[65] The I_{th} was estimated to be 0.95 W cm^{-2} for 488 nm excitation and 2 W cm^{-2} for 532 nm excitation, and this difference in I_{th} is attributed to the larger absorption cross-section of silicon nanoparticles in the short-wavelength region (eqn (9)).[65] When the size of silicon nanoparticles decreased from 3.6 to 3.1 nm, Φ_{UC} increased from 0 to $3.5 \pm 0.5\%$ $(\Phi'_{UC} = 7.0 \pm 0.9\%)$. This occurs because the bandgap increases as the nanoparticle size decreases. When the bandgap exceeds the T_1 energy of 9EA (1.8 eV), efficient TET1 is observed. Further analysis revealed that the triplet excitons generated in silicon nanoparticles undergo Dexter-type TET ($\Phi_{TET1} = 0.48$) to 9EA in approximately 15 ns. Other factors contributing to losses in the TET1 process include the presence of silicon nanoparticles without bound 9EA, the existence of silicon nanoparticles with an excessively small E_g (larger size), and the degradation of silicon nanoparticles. Overcoming these non-uniformity and instability issues may enable TET up to 91% in silicon nanoparticles.[65]

The same research group has recently adopted a novel approach to enhance TET efficiency.[66] Specifically, they modified the binding mode of the anthracene-derived transmitter on the surfaces of silicon nanoparticles from C–C single bonds (Si:9EA) to C=C double bonds (Si:9VA, 9VA = 9-vinylanthracene). This alteration allowed carriers formed in the silicon nanoparticles to delocalize across both the anthracene and silicon nanoparticles, establishing a strongly electronically coupled composite nanosystem. These observations are supported by DFT calculations, indicating that (1) the band-decomposed partial charge density of Si:9VA is significantly broader compared with that of Si:9EA, and (2) the Si:9VA system exhibits a stronger electronic coupling between the anthracene moiety of the transmitter and the silicon nanoparticle, leading to a lower triplet energy compared with that of Si:9EA. In Si:9VA, transient absorption spectroscopy revealed that a new band of triplet states with both characteristics is formed because of the strong electronic coupling between silicon nanoparticles and 9VA. This results in the enhancement of ISC from the singlet excitons localized on the silicon nanoparticles to the newly formed triplet exciton states on a timescale of approximately 3 ns. This suggests that triplet band of Si:9VA can be tuned by adjusting the coordination number of

Fig. 13 (a) Schematic illustration of Si:9EA/DPA and its TTA-UC scheme. Reproduced from ref. 63, with permission from Royal Society of Chemistry, Copyright 2022 (b) Schematic illustration of Si:3EP/tBu$_4$P and its TTA-UC scheme. Reproduced from ref. 64 with permission from Royal Society of Chemistry, Copyright 2021.

9VA, emphasizing the effectiveness of optimizing the coordination number, to obtain efficient triplet sensitization of the desired emitter. When combining the Si:9VA sensitizer that has an optimized average coordination number of 1.8 with a DPA emitter in a solution system (Si:9VA/DPA), a high Φ_{UC} of 1.8% ($\Phi'_{UC} = 3.6\%$) was achieved. Furthermore, for Si:9VA with an average coordination number of 2.9, when combined with a tBu$_4$P emitter, an inner filter effect was considered, resulting in a UC efficiency of 8.6% (17.2% (100% maximum)) and an I_{th} of 0.5 W cm^{-2}.[66]

4. Inorganic nanocluster sensitizers

Nanoclusters are composed of a few to several dozen atoms, making them smaller than nanoparticles, and have been studied since the early 1980s, primarily obtained through vacuum-based gas-phase experiments.[67,68] Notably, fullerene, known for a Φ_{ISC} of ~100%, is a carbon nanocluster. In the late 1990s, stable handling of metal nanoclusters under atmospheric conditions became feasible by protecting them with ligands, and in the 2000s, various precise synthetic methods were established in liquid phases. The molecular structures of ligand-protected metal nanoclusters composed of noble metals such as gold, silver, and platinum have been revealed through single-crystal X-ray structural analysis, with numerous reported examples.[69–72] Thus, ligand-protected metal nanoclusters represent well-structured and defined systems that enable precise control of size and composition. Furthermore, scaling laws do not apply to these substances, and even a one-atom difference in composition significantly influences their structure and properties.[73]

Mitsui and colleagues discovered that ligand-protected metal nanoclusters can sensitize the triplet states of fluorescent dyes, leading to the exploration of metal nanoclusters in TTA-UC studies. The first observation of triplet sensitization occurred in a mixed system of thiolate-protected silver and platinum-containing MAg$_{24}$ nanoclusters ([PPh$_4$]$_n$[MAg$_{24}$(DMBT)$_{18}$], (M, n) = (Ag, 1), (Pt, 2)) with perylene and TIPS-anthracene (TIPS-Ac) (PPh$_4$ = tetraphenylphosphonium ion, DMBT = 2,4-dimethylbenzenethiolate), reported in 2020.[74] Both Ag$_{25}$ and PtAg$_{24}$ exhibit a structure where a central M atom is surrounded by an icosahedral Ag$_{12}$ core covered by six [Ag$_2$(DMBT)$_3$] oligomers (Fig. 14(a)).[72,75] When these MAg$_{24}$ nanoclusters were mixed with fluorescent dyes and excited with 640 nm light under deoxygenated conditions, UC emission was observed for both solution samples. The TET efficiency of PtAg$_{24}$/emitter (K_{SV} ~300 M^{-1}, k_{TET} ~2 × 10^8 s^{-1}) was significantly higher than that of Ag$_{25}$/emitter (K_{SV} ~16 M^{-1}, k_{TET} ~1.5 × 10^7 s^{-1}), attributed to the lower absorption energy in Ag$_{25}$, resulting in a smaller driving force for TET. Blue UC photon was observed in the mixed solution of MAg$_{24}$/emitter under deoxygenated conditions upon 640 nm excitation, and the quantum yield (Φ_{UC} ~1%) of PtAg$_{24}$/emitter was orders of magnitude higher than that of Ag$_{25}$/emitter (Φ_{UC} ~10^{-4}%) (Fig. 14(b) and (c)). However, the reason for this discrepancy could not be solely explained by TET efficiency. Therefore, the authors undertook an analysis of the triplet generation efficiency of metal nanoclusters, which was previously unclear, by considering the loss processes in
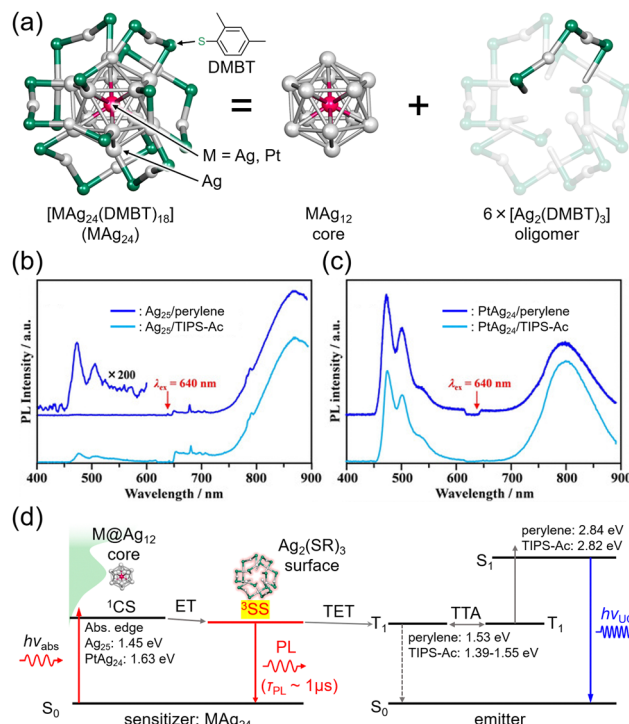

Fig. 14 (a) Schematic illustration of MAg$_{24}$ (M = Ag, Pt). (b) and (c) Photoluminescence spectra for deaerated solution of Ag$_{25}$/emitter and PtAg$_{24}$/emitter (emitter = perylene or TIPS-Ac), respectively, excited by 640 nm. (d) Relaxation process of excited MAg$_{24}$ and energy diagram of TTA-UC in the MAg$_{24}$/emitter system. Reproduced from ref. 74 with permission from Wiley-VCH GmbH, Copyright 2020.

UC (self-absorption and sensitizer-induced deactivation of ^{3}Em*), in a TTA-UC framework.[19] As a result, the triplet generation efficiency of PtAg$_{24}$ was found to be approximately 230 times larger than that of Ag$_{25}$. For such thiolate-protected metal nanoclusters, a model has been proposed, suggesting that the core is responsible for light absorption, with the excited energy rapidly moving to the surface, where the oligomers emit light (Fig. 14(d)).[76,77] The authors interpreted the triplet generation efficiency obtained from TTA-UC analysis as the efficiency of surface triplet excitations, proposing a deactivation model for MAg$_{24}$. Consequently, the luminescence was attributed to phosphorescence from the surface. Moreover, by optimizing the system, the team achieved UC from 785 nm NIR light to blue light with a ΔE_{AS} exceeding 1 eV in both the solution and solid states, marking the first example of exciting the T$_1$ state of perylene with 785 nm NIR light.[74]

Other cluster with icosahedral Ag$_{12}$ cores doped with Pt, [Ag$_{28}$Pt(BDT)$_{12}$(PPh$_4$)$_4$]$^{4-}$, has also been reported by Bakr $et\ al.$ This cluster has a PtAg$_{12}$ core protected by Ag$_{16}$(BDT)$_{12}$ ligand shell composed of Ag and dithiolate (1,3-benzenedithiolate) and PPh$_3$.[78] Mitsui $et\ al.$ evaluated the excited state and TTA-UC properties of a PtAg$_{28}$ cluster ([PtAg$_{28}$(BDT)$_{12}$]$^{4-}$) without the secondary ligand, PPh$_3$. Quantum chemical calculations showed that the electron configuration of S$_1$ and T$_1$ in PtAg$_{28}$ is similar, which results in a smaller matrix element of the spin–orbit coupling between S$_1$ and T$_1$, slowing down these

ISCs. On the other hand, there is a T_2 level capable of direct SOC at energies lower than S_1, and a highly efficient T_1 state is formed by the $S_1 \rightarrow T_2 \rightarrow T_1$ pathway ($\Phi_{ISC} \sim 1$). The resulting T_1 state has charge transfer properties from the $PtAg_{12}$ core to the surface, giving it excellent sensitization ability; $PtAg_{28}$, in combination with DPA, achieves TTA-UC from 532 nm excitation light to blue ($\Delta E_{AS} = 0.52$ eV) with a Φ_{UCg} of 12.2% and its I_{th} recorded an extremely low value of 0.81 mW cm^{-2}.[79]

The icosahedral 13-atom metal core is commonly observed in ligand-protected metal nanoclusters, not limited to MAg_{24} mentioned earlier.[80] Among them, the Au_{13} nanocluster protected by diphosphine and halogen, $[Au_{13}(dppe)_5Cl_2]^{3+}$ (dppe = 1,2-bis(diphenylphosphino)ethane), stands out as one of the most well-known gold nanoclusters (Fig. 15(a)).[81–86] Because the molecular orbitals of such ligand-protected metal nanoclusters have analogous shapes to atomic orbitals (s, p, d,...), they are often referred to as "superatoms," and their molecular orbitals are termed "superatomic orbitals" (S, P, D,...). In recent years, it has been demonstrated that the Au_{13} nanocluster in the Au_{13}/perylene solution system undergoes TTA-UC from red (640 nm) to blue (472 nm), revealing the ability of the Au_{13} nanocluster to sensitize the T_1 state of perylene (Fig. 15(b)–(d)).[87] Furthermore, the mechanism of triplet state generation in these Au_{13} nanoclusters has been elucidated through the understanding of superatomic orbitals.[88]
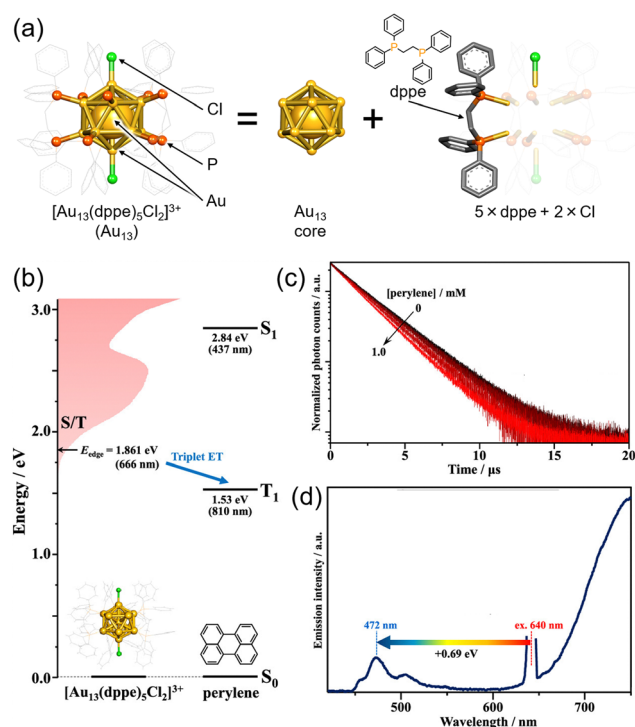
The rod-shaped nanocluster rod-Au_{25}, first reported by Tsukuda et al., has a shared gold atom from two icosahedral Au_{13}. One of these rod-Au_{25} clusters, $[Au_{25}(PPh_3)_{10}(PET)_5Cl_2](SbF_6)_2$ (PPh$_3$ = triphenylphosphine, PET = 2-phenylethanethiolate, SbF$_6$ = hexafluoroantimonate ion) (Fig. 16(a)),[89–92] also exhibits TTA-UC characteristics when combined with BPEA (9,10-bis(phenylethynyl)anthracene) or rubrene (Fig. 16(b)–(d)). Owing to its longer-wavelength absorption compared with Au_{13}, rod-Au_{25} is anticipated to display NIR TTA-UC.[93] Furthermore, rod-Au_{25} nanoclusters have an Φ_{ISC} of nearly 1, making them suitable as phosphorescent materials with a dark S_1 state and bright T_1 state at room temperature. Similar to other ligand-protected metal nanoclusters, the electronic structure of rod-Au_{25} can be modified by substituting different metal atoms.[94–105] Alloyed rod-$Au_{25-x}Ag_x$ exhibits unique properties; for $0 \leq x \leq 12$, the photoluminescence quantum yield is low, but at $x = 13$, there is a sudden and significant increase, approximately 200-fold.[106] Mitsui and colleagues conducted TTA-UC analysis of rod-$Au_{25-x}Ag_x$/perylene, revealing the following key findings: (1) photoluminescence from $Au_{25-x}Ag_x$ is phosphorescent, (2) $x = 12$ may have the same high photoluminescence quantum yield as $x = 13$, and (3) substituting Ag atoms in the connecting part of the icosahedral core results in a higher energy shift of the triplet energy and enhancement of phosphorescence.[107]

The Au_2Cu_6 nanocluster reported by Zhu and colleagues, $[Au_2Cu_6(S\text{-}Adm)_6(PPh_3)_2]$ (S-Adm = 1-adamantanethiolate) (Fig. 17(a) and (c)), features a highly symmetric structure, with a cyclic copper-thiolate oligomer $[Cu\text{-}S(\text{-}Adm)\text{-}]_6$ surrounding an

Fig. 15 (a) Schematic illustration of Au_{13}. (b) Energy-level diagram of Au_{13} and perylene. (b) Photoluminescence decay curves of Au_{13} in deaerated solvent using 634 nm excitation. (c) Photoluminescence spectrum obtained for the deaerated solution of Au_{13}/perylene using 640 nm CW laser excitation. Reproduced from ref. 85 with permission from American Chemical Society, Copyright 2022.
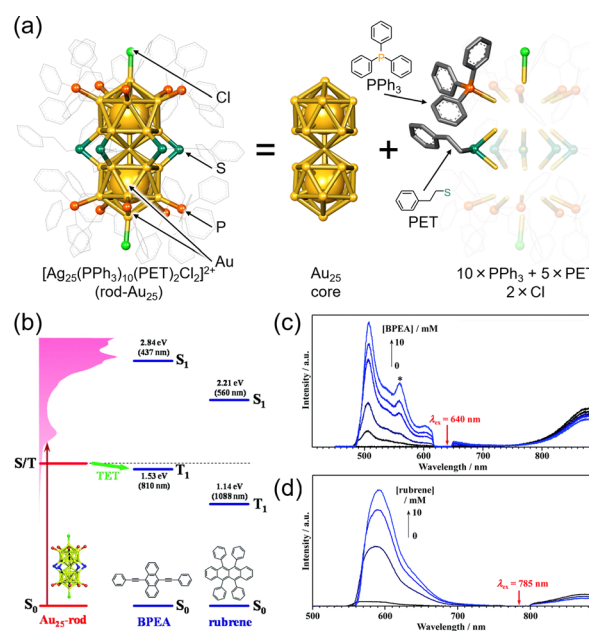

Fig. 16 (a) Schematic illustration of rod-Au_{25}. (b) Energy-level diagram of the Au_{25}, BPEA and rubrene. (c) Photoluminescence spectra obtained for the deaerated solution of Au_{25}/BPEA using 640 nm excitation. (d) Photoluminescence spectra obtained for the deaerated solution of rod-Au_{25}/rubrene using 785 nm excitation. Reproduced from ref. 93 with permission from Royal Society of Chemistry, Copyright 2022.
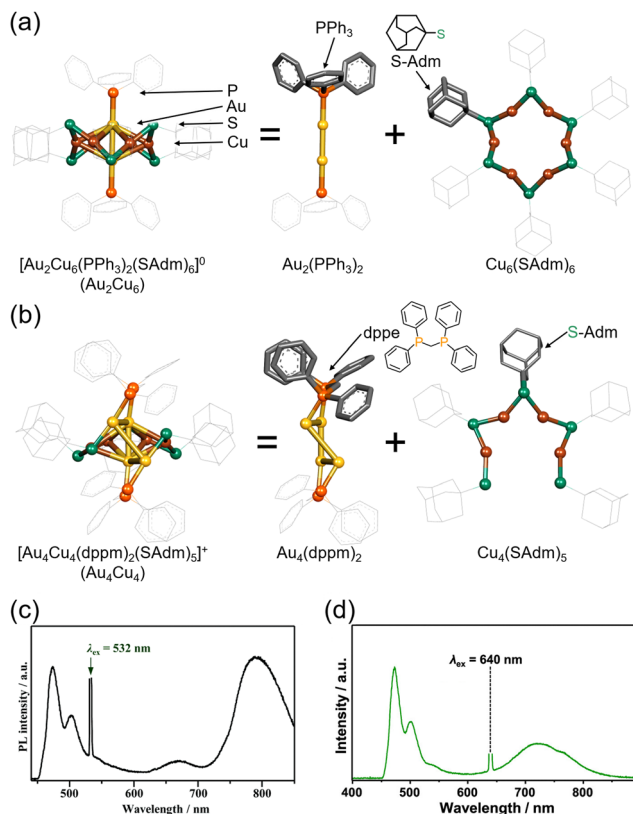
Fig. 17 (a) Schematic illustration of Au_2Cu_6. (b) Schematic illustration of Au_4Cu_4. (c) Photoluminescence spectrum obtained for the deaerated solution of Au_2Cu_6/perylene with the 532 nm CW laser excitation. Reproduced from ref. 110 with permission from Royal Society of Chemistry, Copyright 2022. (d) Photoluminescence spectrum obtained for the deaerated solution of Au_4Cu_4/perylene with the 640 nm CW laser excitation. Reproduced from ref. 112 with permission from American Chemical Society, Copyright 2023.

upper and lower PPh_3-coordinated Au_2 dimer.[108,109] Mitsui and coworkers discovered that this Au_2Cu_6 nanocluster exhibits the rare ability to simultaneously emit both fluorescence and phosphorescence. Using platinum(II) octaethylporphine (PtOEP) and perylene in solution (PtOEP/perylene) as a reference system, they estimated the Φ_{ISC} of Au_2Cu_6 to be 0.47.[110] Additionally, detailed excitation relaxation processes of Au_2Cu_6 nanoclusters were revealed by temperature-dependent luminescence spectroscopy, marking the first instance of detailed experimental insight into the excitation relaxation processes of metal nanoclusters.[110]

The research group also conducted TTA-UC analysis for an Au_4Cu_4 nanocluster, $[Au_4Cu_4(dppm)_2(S-Adm)_5]Cl$ (dppm = 1,1-bis(diphenylphosphino)methane) (Fig. 17(b) and (d)),[111] elucidating the detailed excited states of this nanocluster.[112] Although Au_4Cu_4 and Au_2Cu_6 exhibit similar absorption spectra, fluorescence was not observed in Au_4Cu_4. TTA-UC analysis was performed using 640 nm excitation light with perylene or DPA, and Φ_{ISC} for Au_4Cu_4 was estimated to be 0.97. Upon estimating the activation barrier between S_1 and T_1, the activation barrier for Au_4Cu_4 was determined to be 4.8 meV, significantly lower compared to that for Au_2Cu_6 (250 meV). Analysis of

excited states through DFT calculations for both singlet and triplet state of Au_4Cu_4 revealed the presence of isoenergetically isomers with slightly different ring structures formed by four Au atoms. Since the matrix elements for ISC between the same isomers are zero, ISC processes without structural changes are less favorable, whereas ISC accompanied by flexible structural changes between isomers is feasible. The ISC rate constant in this model was estimated by employing Marcus semiclassical electron transfer theory, which closely reproduced the experimental values. Therefore, the authors propose that the flexibility in such structural arrangements of Au_4Cu_4 enhances ISC. Au_4Cu_4 exhibits a longer photoluminescence lifetime compared with Au_2Cu_6, and its Φ_{UC} is remarkably high at 14% $(\Phi'_{UC} = 28\%)$, with a low threshold intensity $(I_{th} = 26\ mW\ cm^{-2})$, demonstrating its efficiency as a UC material.[112]

As described above, many ligand-protected metal nanoclusters can function as sensitizers for the triplet states of fluorescent dyes, and these nanoclusters are being recognized as potential sensitizers for TTA-UC, similar to inorganic nanoparticles. However, the electronic states related to the luminescence of ligand-protected metal nanoclusters have not been fully elucidated. For example, the radiative lifetimes are calculated to be in the range of tens to hundreds of microseconds. This uncertainty, along with other factors, contributes to the lack of fundamental knowledge, making it difficult to determine whether the luminescence of nanoclusters is fluorescence or phosphorescence.

Notably, TTA-UC analysis provides optical and photophysical insights related to the excited states of these metal nanoclusters. This aspect is of great interest, both industrially and academically, because it helps clarify the fundamental nature of nanocluster luminescence.

5. Conclusions and perspectives

This review focuses on the recent research in TTA-UC, with an emphasis on studies using inorganic nanomaterials, such as semiconductor nanoparticles, nanocrystals, and ligand-protected metal nanoclusters, as triplet sensitizers, and introduces the concepts of triplet sensitization, TTA-UC characteristics, and the insights derived from these studies.

The physical properties of inorganic nanoparticles and nanocrystals follow scaling law based on particle size, allowing for a reasonable prediction of electronic structure from particle size. Their stability, simplicity of synthesis, and potential for large-scale industrial production make them promising sensitizers. In TTA-UC with inorganic nanoparticles, changes in the bandgap associated with variations in particle size significantly affect the TET efficiency. The development of efficient transmitter ligands capable of effectively transferring triplet energy to emitter molecules has also progressed. In the case of inorganic nanoparticles, UC of NIR excitation light (around 1 μm) to visible light has been achieved.

Moreover, ligand-protected metal nanoclusters offer the advantage of precise control over the number of constituent

atoms and structure during synthesis, allowing for the discussion of obtained properties from a chemical composition and structural perspective. However, breaking the scaling law for physical properties makes it difficult to establish a clear methodology for achieving the desired triplet sensitization and TTA-UC characteristics. Recent efforts have focused on using TTA-UC to determine optical and photophysical parameters, shedding light on the excited-state characteristics of these metal nanoclusters. For instance, photoluminescence spectroscopy provides high sensitivity, making it a promising technique for elucidating the excited-state properties in the future.

6. Outlook

Development of highly efficient UC materials from IR/NIR to visible light

Both inorganic nanoparticles and ligand-protected metal nanoclusters consist of quantum-confined metal or semiconductor cores, as well as ligands. These materials are highly photostable and exhibit strong light absorption, even in the NIR region, making them attractive for efficient NIR light absorbers and triplet sensitizers. In the future, the development of nanomaterial-based systems capable of upconverting longer-wavelength IR/NIR light to visible light is anticipated.

Development of nanomaterials with visible range transparency

Both inorganic nanoparticles and ligand-protected metal nanoclusters exhibit increased absorption cross-sections with shorter wavelengths, enhancing the reabsorption of UC photon generated by TTA-UC. While reabsorption can be mitigated through various methods, such as shortening the light path of UC photons or solid-state thin film formation, for inorganic nanomaterials, it may also be possible to design molecules that suppress reabsorption by ensuring lower absorption efficiency of the nanomaterial in the emission wavelength range of the emitter. For example, gold nanoclusters, such as $[Au_{37}(PPh_3)_{10}(PET)_{10}X_2]^+$ (X = halogen), $Au_{42}(PET)_{32}$, and $Ag_{14}(1,2\text{-}BDT)_6(PPh_3)_8$ (1,3-BDT = 1,3-benzenedithiolate) reported by Jin and Pradeep, exhibit absorption in the NIR region but high light transparency in the visible range.[113–115] Such absorption behavior, similar to that of metal porphyrins, may enable TTA-UC with suppressed optical loss.

Development of highly efficient triplet sensitizers using metal nanoclusters: trans systems

Metal nanoclusters can be modified post-synthesis using various methods, such as ligand exchange, allowing for the introduction of desired ligands.[116] Consequently, it is anticipated that metal nanoclusters can be complexed with dye ligands.[117–128] Moreover, recent separation techniques enable the isolation of metal nanoclusters based on the number of introduced ligands or isomers.[129–133] Therefore, quantitative insights into how TET and UC properties change depending on the number and position of introduced ligands may be elucidated. For such well-defined systems, the integration of quantum chemical calculations is anticipated to provide a deeper understanding of the observed phenomena.

Reduction of energy loss through the development of metal nanoclusters: emitter/emitter systems

The use of molecules acting as both transmitter ligands and emitter molecules for nanoclusters, such as TES-ADT and PPO in nanoparticle systems, is an effective means to suppress energy loss in the energy cascade of TTA-UC.[51,57] For certain ligand-protected metal nanoclusters, such as $[Ag_{29}(BDT)_{12}\text{-}(PPh_3)_4]^{3-}$ and $[Ag_{51}(BDT)_{19}(PPh_3)_3]^{3-}$ (BDT = 1,3-benzenedithiolate), it has been revealed that the secondary ligand, phosphine, is in a dynamic equilibrium state of binding and dissociation in solution.[134–138] These metal nanoclusters may exhibit the aforementioned energy loss suppression effect. In the future, the TTA-UC phenomena demonstrated by these nanoclusters may be elucidated, and with the use of ligand selection and dynamic equilibrium states, numerous metal nanoclusters with such suppression effects can be created.

Development of nanoparticle: nanocluster/emitter systems

To achieve TTA-UC in the NIR range, it is necessary to develop transmitters with lower T_1 energy. The extension of the π-conjugated system in organic systems leads to a decrease in photostability, suggesting limitations in achieving such development with organic dye systems. In contrast, metal nanoclusters exhibit high photostability and low T_1 energy. Furthermore, carboxyl groups or acene-based substituents can be applied on the nanocluster surface through ligand-exchange reactions. Novel composite materials formed by coordinating such metal nanoclusters as transmitters on the surfaces of inorganic nanoparticles are expected to overcome the weaknesses of conventional organic transmitter-based composites.

Author contributions

Y. Niihori: conceptualization, information collection, writing (original draft and editing). T, Kosaka: information collection, writing (original draft). Y. Negishi: conceptualization, writing (editing), supervision, project administration.

Conflicts of interest

There are no conflicts of interest to declare.

Acknowledgements

References

1 V. C. Gordon, *Man Makes Himself*, Watts & Co., London, 1936.

2 Y. Wang, K. Zheng, S. Song, D. Fan, H. Zhang and X. Liu, *Chem. Soc. Rev.*, 2018, **47**, 6473.

3 S. Borse, R. Rafique, Z. V. P. Murthy, T. J. Park and S. K. Kailasa, *Analyst*, 2022, **147**, 3155.

4 D. R. Gamelin and H. U. Güdel, *Acc. Chem. Res.*, 2000, **33**, 235.

5 J. C. Goldschmidt and S. Fischer, *Adv. Opt. Mater.*, 2015, **3**, 510.

6 J. Zhou, Q. Liu, W. Feng, Y. Sun and F. Li, *Chem. Rev.*, 2015, **115**, 395.

7 V. Yakutkin, S. Aleshchenkov, S. Chernov, T. Miteva, G. Nelles, A. Cheprakov and S. Baluschev, *Chem. – Eur. J.*, 2008, **14**, 9846.

8 L. Zeng, L. Huang, J. Han and G. Han, *Acc. Chem. Res.*, 2022, **55**, 2604.

9 S. E. Seo, H.-S. Choe, H. Cho, H.-I. Kim, J.-H. Kim and O. S. Kwon, *J. Mater. Chem. C*, 2022, **10**, 4483.

10 M. Uji, T. J. B. Zähringer, C. Kerzig and N. Yanai, *Angew. Chem., Int. Ed.*, 2023, **62**, e202301506.

11 Y. Sasaki, S. Amemori, N. Yanai and N. Kimizuka, *Bull. Chem. Soc. Jpn.*, 2021, **94**, 1760.

12 P. Bharmoria, H. Bildirir and K. Moth-Poulsen, *Chem. Soc. Rev.*, 2020, **49**, 6529.

13 L. Naimovičius, P. Bharmoria and K. Moth-Poulsen, *Mater. Chem. Front.*, 2023, **7**, 2297.

14 L. Wei, C. Yang and W. Wu, *Mater. Chem. Front.*, 2023, **7**, 3194.

15 A. Ronchi, P. Brazzo, M. Sassi, L. Beverina, J. Pedrini, F. Meinardi and A. Monguzzi, *Phys. Chem. Chem. Phys.*, 2019, **21**, 12353.

16 A. Ronchi and A. Monguzzi, *Chem. Phys. Rev.*, 2022, **3**, 041301.

17 C. A. Parker, C. G. Hatchard and E. J. Bowen, *Proc. R. Soc. London, Ser. A*, 1962, **269**, 574.

18 N. Yanai, K. Suzuki, T. Ogawa, Y. Sasaki, N. Harada and N. Kimizuka, *J. Phys. Chem. A*, 2019, **123**, 10197.

19 Y. Zhou, F. N. Castellano, T. W. Schmidt and K. Hanson, *ACS Energy Lett.*, 2020, **5**, 2322.

20 T. N. Singh-Rachford and F. N. Castellano, *J. Phys. Chem. Lett.*, 2010, **1**, 195.

21 Z. Huang and M. L. Tang, *J. Am. Chem. Soc.*, 2017, **139**, 9412.

22 S. M. Bachilo and R. B. Weisman, *J. Phys. Chem. A*, 2000, **104**, 7711.

23 Y. Y. Cheng, B. Fückel, T. Khoury, R. G. C. R. Clady, M. J. Y. Tayebjee, N. J. Ekins-Daukes, M. J. Crossley and T. W. Schmidt, *J. Phys. Chem. Lett.*, 2010, **1**, 1795.

24 F. Edhborg, A. Olesund and B. Albinsson, *Photochem. Photobiol. Sci.*, 2022, **21**, 1143.

25 Y. Murakami, *Chem. Phys. Lett.*, 2011, **516**, 56.

26 K. Kamada, Y. Sakagami, T. Mizokuro, Y. Fujiwara, K. Kobayashi, K. Narushima, S. Hirata and M. Vacha, *Mater. Horiz.*, 2017, **4**, 83.

27 A. Abulikemu, Y. Sakagami, C. Heck, K. Kamada, H. Sotome, H. Miyasaka, D. Kuzuhara and H. Yamada, *ACS Appl. Mater. Interfaces*, 2019, **11**, 20812.

28 A. Monguzzi, J. Mezyk, F. Scotognella, R. Tubino and F. Meinardi, *Phys. Rev. B: Condens. Matter Mater. Phys.*, 2008, **78**, 195112.

29 A. I. Ekimov and A. A. Onushchenko, *JETP Lett.*, 2023, **118**, S15.

30 R. Rossetti and L. Brus, *J. Phys. Chem.*, 1982, **86**, 4470.

31 C. B. Murray, D. J. Norris and M. G. Bawendi, *J. Am. Chem. Soc.*, 1993, **115**, 8706.

32 S. Katharine and C. Davide, *Nature*, 2023, **622**, 2.

33 A. Khetubol, S. Van Snick, A. Hassinen, E. Fron, Y. Firdaus, L. Pandey, C. C. David, K. Duerinckx, W. Dehaen, Z. Hens and M. Van der Auweraer, *J. Appl. Phys.*, 2013, **113**, 083507.

34 A. Monguzzi, D. Braga, M. Gandini, V. C. Holmberg, D. K. Kim, A. Sahu, D. J. Norris and F. Meinardi, *Nano Lett.*, 2014, **14**, 6644.

35 Z. Huang, X. Li, M. Mahboub, K. M. Hanson, V. M. Nichols, H. Le, M. L. Tang and C. J. Bardeen, *Nano Lett.*, 2015, **15**, 5552.

36 M. Mahboub, H. Maghsoudiganjeh, A. M. Pham, Z. Huang and M. L. Tang, *Adv. Funct. Mater.*, 2016, **26**, 6091.

37 Z. Huang, X. Li, B. D. Yip, J. M. Rubalcava, C. J. Bardeen and M. L. Tang, *Chem. Mater.*, 2015, **27**, 7503.

38 G. B. Piland, Z. Huang, M. Lee Tang and C. J. Bardeen, *J. Phys. Chem. C*, 2016, **120**, 5883.

39 P. Xia, Z. Huang, X. Li, J. J. Romero, V. I. Vullev, G. S. H. Pau and M. L. Tang, *Chem. Commun.*, 2017, **53**, 1241.

40 J. Zhang, H. Kouno, N. Yanai, D. Eguchi, T. Nakagawa, N. Kimizuka, T. Teranishi and M. Sakamoto, *ACS Photonics*, 2020, **7**, 1876.

41 X. Li, Z. Huang, R. Zavala and M. L. Tang, *J. Phys. Chem. Lett.*, 2016, **7**, 1955.

42 Z. Huang, Z. Xu, T. Huang, V. Gray, K. Moth-Poulsen, T. Lian and M. L. Tang, *J. Am. Chem. Soc.*, 2020, **142**, 17581.

43 X. Li, A. Fast, Z. Huang, D. A. Fishman and M. L. Tang, *Angew. Chem., Int. Ed.*, 2017, **56**, 5598.

44 J. De Roo, Z. Huang, N. J. Schuster, L. S. Hamachi, D. N. Congreve, Z. Xu, P. Xia, D. A. Fishman, T. Lian, J. S. Owen and M. L. Tang, *Chem. Mater.*, 2020, **32**, 1461.

45 Z. Huang, D. E. Simpson, M. Mahboub, X. Li and M. L. Tang, *Chem. Sci.*, 2016, **7**, 4101.

46 Z. Huang, Z. Xu, M. Mahboub, Z. Liang, P. Jaimes, P. Xia, K. R. Graham, M. L. Tang and T. Lian, *J. Am. Chem. Soc.*, 2019, **141**, 9769.

47 J. A. Bender, E. K. Raulerson, X. Li, T. Goldzak, P. Xia, T. Van Voorhis, M. L. Tang and S. T. Roberts, *J. Am. Chem. Soc.*, 2018, **140**, 7543.

48 J. Zhang, H. Sakai, K. Suzuki, T. Hasobe, N. V. Tkachenko, I. Y. Chang, K. Hyeon-Deuk, H. Kaji, T. Teranishi and M. Sakamoto, *J. Am. Chem. Soc.*, 2021, **143**, 17388.

49 H. Sakai, R. Inaya, N. V. Tkachenko and T. Hasobe, *Chem. – Eur. J.*, 2018, **24**, 17062.

50 Z. Xu, T. Jin, Y. Huang, K. Mulla, F. A. Evangelista, E. Egap and T. Lian, *Chem. Sci.*, 2019, **10**, 6120.

51 N. Nishimura, J. R. Allardice, J. Xiao, Q. Gu, V. Gray and A. Rao, *Chem. Sci.*, 2019, **10**, 4750.

52 M. Wu, D. N. Congreve, M. W. B. Wilson, J. Jean, N. Geva, M. Welborn, T. Van Voorhis, V. Bulović, M. G. Bawendi and M. A. Baldo, *Nat. Photonics*, 2016, **10**, 31.

53 N. Tripathi and K. Kamada, *ACS Appl. Nano Mater.*, 2024, **7**, 2950.

54 M. Mahboub, Z. Huang and M. L. Tang, *Nano Lett.*, 2016, **16**, 7169.

55 Z. Huang, Z. Xu, M. Mahboub, X. Li, J. W. Taylor, W. H. Harman, T. Lian and M. L. Tang, *Angew. Chem., Int. Ed.*, 2017, **56**, 16583.

56 M. Mahboub, P. Xia, J. Van Baren, X. Li, C. H. Lui and M. L. Tang, *ACS Energy Lett.*, 2018, **3**, 767.

57 V. Gray, P. Xia, Z. Huang, E. Moses, A. Fast, D. A. Fishman, V. I. Vullev, M. Abrahamsson, K. Moth-Poulsen and M. Lee Tang, *Chem. Sci.*, 2017, **8**, 5488.

58 K. Mase, K. Okumura, N. Yanai and N. Kimizuka, *Chem. Commun.*, 2017, **53**, 8261.

59 K. Okumura, N. Yanai and N. Kimizuka, *Chem. Lett.*, 2019, **48**, 1347.

60 M. Koharagi, N. Harada, K. Okumura, J. Miyano, S. Hisamitsu, N. Kimizuka and N. Yanai, *Nanoscale*, 2021, **13**, 19890.

61 N. Gong, R. Lai, S. Xing, Z. Liu, J. Mo, T. Man, Z. Li, D. Di, J. Du, D. Tan, X. Liu, J. Qiu and B. Xu, *Adv. Sci.*, 2023, **10**, 2305069.

62 K. Leung and K. B. Whaley, *Phys. Rev. B: Condens. Matter Mater. Phys.*, 1997, **56**, 7455.

63 J. Schwan, K. Wang, M. L. Tang and L. Mangolini, *Nanoscale*, 2022, **14**, 17385.

64 T. Huang, T. T. Koh, J. Schwan, T. T. T. Tran, P. Xia, K. Wang, L. Mangolini, M. L. Tang and S. T. Roberts, *Chem. Sci.*, 2021, **12**, 6737.

65 P. Xia, E. K. Raulerson, D. Coleman, C. S. Gerke, L. Mangolini, M. L. Tang and S. T. Roberts, *Nat. Chem.*, 2020, **12**, 137.

66 K. Wang, R. P. Cline, J. Schwan, J. M. Strain, S. T. Roberts, L. Mangolini, J. D. Eaves and M. L. Tang, *Nat. Chem.*, 2023, **15**, 1172.

67 W. A. de Heer, *Rev. Mod. Phys.*, 1993, **65**, 611.

68 M. L. Cohen and W. D. Knight, *Phys. Today*, 1990, **43**, 42.

69 P. D. Jadzinsky, G. Calero, C. J. Ackerson, D. A. Bushnell and R. D. Kornberg, *Science*, 2007, **318**, 430.

70 M. Zhu, C. M. Aikens, F. J. Hollander, G. C. Schatz and R. Jin, *J. Am. Chem. Soc.*, 2008, **130**, 5883.

71 M. W. Heaven, A. Dass, P. S. White, K. M. Holt and R. W. Murray, *J. Am. Chem. Soc.*, 2008, **130**, 3754.

72 C. P. Joshi, M. S. Bootharaju, M. J. Alhilaly and O. M. Bakr, *J. Am. Chem. Soc.*, 2015, **137**, 11578.

73 Y. Negishi, K. Nobusada and T. Tsukuda, *J. Am. Chem. Soc.*, 2005, **127**, 5261.

74 Y. Niihori, Y. Wada and M. Mitsui, *Angew. Chem., Int. Ed.*, 2021, **60**, 2822.

75 X. Kang, M. Zhou, S. Wang, S. Jin, G. Sun, M. Zhu and R. Jin, *Chem. Sci.*, 2017, **8**, 2581.

76 M. S. Bootharaju, C. P. Joshi, M. R. Parida, O. F. Mohammed and O. M. Bakr, *Angew. Chem., Int. Ed.*, 2016, **55**, 922.

77 M. Zhou, H. Qian, M. Y. Sfeir, K. Nobusada and R. Jin, *Nanoscale*, 2016, **8**, 7163.

78 M. S. Bootharaju, S. M. Kozlov, Z. Cao, M. Harb, M. R. Parida, M. N. Hedhili, O. F. Mohammed, O. M. Bakr, L. Cavallo and J.-M. Basset, *Nanoscale*, 2017, **9**, 9529.

79 M. Mitsui and A. Uchida, *Nanoscale*, 2024, **16**, 3053.

80 C. E. Briant, B. R. C. Theobald, J. W. White, L. K. Bell, D. M. P. Mingos and A. J. Welch, *J. Chem. Soc., Chem. Commun.*, 1981, 201.

81 Y. Shichibu and K. Konishi, *Small*, 2010, **6**, 1216.

82 H. Hirai, T. Nakashima, S. Takano, Y. Shichibu, K. Konishi, T. Kawai and T. Tsukuda, *J. Mater. Chem. C*, 2023, **11**, 3095.

83 H. Hirai, S. Takano, T. Nakashima, T. Iwasa, T. Taketsugu and T. Tsukuda, *Angew. Chem., Int. Ed.*, 2022, **61**, e202207290.

84 Y. Shichibu, Y. Ogawa, M. Sugiuchi and K. Konishi, *Nanoscale Adv.*, 2021, **3**, 1005.

85 H. Hirai, S. Takano, T. Nakamura and T. Tsukuda, *Inorg. Chem.*, 2020, **59**, 17889.

86 M. R. Narouz, S. Takano, P. A. Lummis, T. I. Levchenko, A. Nazemi, S. Kaappa, S. Malola, G. Yousefalizadeh, L. A. Calhoun, K. G. Stamplecoskie, H. Häkkinen, T. Tsukuda and C. M. Crudden, *J. Am. Chem. Soc.*, 2019, **141**, 14997.

87 M. Mitsui, D. Arima, A. Uchida, K. Yoshida, Y. Arai, K. Kawasaki and Y. Niihori, *J. Phys. Chem. Lett.*, 2022, **13**, 9272.

88 K. Yoshida, D. Arima and M. Mitsui, *J. Phys. Chem. Lett.*, 2023, **14**, 10967.

89 Y. Shichibu, Y. Negishi, T. Watanabe, N. K. Chaki, H. Kawaguchi and T. Tsukuda, *J. Phys. Chem. C*, 2007, **111**, 7845.

90 Y. Niihori, S. Miyajima, A. Ikeda, T. Kosaka and Y. Negishi, *Small Sci.*, 2023, **3**, 2300024.

91 M. Galchenko, R. Schuster, A. Black, M. Riedner and C. Klinke, *Nanoscale*, 2019, **11**, 1988.

92 H. Qian, W. T. Eckenhoff, M. E. Bier, T. Pintauer and R. Jin, *Inorg. Chem.*, 2011, **50**, 10735.

93 M. Mitsui, Y. Wada, R. Kishii, D. Arima and Y. Niihori, *Nanoscale*, 2022, **14**, 7974.

94 Y. Negishi, T. Iwai and M. Ide, *Chem. Commun.*, 2010, **46**, 4713.

95 Y. Negishi, W. Kurashige, Y. Niihori, T. Iwasa and K. Nobusada, *Phys. Chem. Chem. Phys.*, 2010, **12**, 6219.

96 Y. Negishi, K. Munakata, W. Ohgake and K. Nobusada, *J. Phys. Chem. Lett.*, 2012, **3**, 2209.

97 H. Qian, D.-e Jiang, G. Li, C. Gayathri, A. Das, R. R. Gil and R. Jin, *J. Am. Chem. Soc.*, 2012, **134**, 16159.

98 S. Wang, Y. Song, S. Jin, X. Liu, J. Zhang, Y. Pei, X. Meng, M. Chen, P. Li and M. Zhu, *J. Am. Chem. Soc.*, 2015, **137**, 4018.

99 M. Jash, A. Jana, A. K. Poonia, E. Khatun, P. Chakraborty, A. Nagar, T. Ahuja, K. V. Adarsh and T. Pradeep, *Chem. Mater.*, 2023, **35**, 313.

100 Z. Liu, M. Zhou, L. Luo, Y. Wang, E. Kahng and R. Jin, *J. Am. Chem. Soc.*, 2023, **145**, 19969.

101 A. Ghosh, O. F. Mohammed and O. M. Bakr, *Acc. Chem. Res.*, 2018, **51**, 3094.

102 K. H. Wijesinghe, N. A. Sakthivel, T. Jones and A. Dass, *J. Phys. Chem. Lett.*, 2020, **11**, 6312.

103 R.-W. Huang, X. Song, S. Chen, J. Yin, P. Maity, J. Wang, B. Shao, H. Zhu, C. Dong, P. Yuan, T. Ahmad, O. F. Mohammed and O. M. Bakr, *J. Am. Chem. Soc.*, 2023, **145**, 13816.

104 T.-H. Chiu, J.-H. Liao, F. Gam, I. Chantrenne, S. Kahlal, J.-Y. Saillard and C. W. Liu, *J. Am. Chem. Soc.*, 2019, **141**, 12957.

105 J.-H. Liao, T.-H. Chiu, H. Liang, S. Kahlal, J.-Y. Saillard and C. W. Liu, *Nanoscale*, 2023, **15**, 6121.

106 S. Wang, X. Meng, A. Das, T. Li, Y. Song, T. Cao, X. Zhu, M. Zhu and R. Jin, *Angew. Chem., Int. Ed.*, 2014, **53**, 2376.

107 M. Mitsui, D. Arima, Y. Kobayashi, E. Lee and Y. Niihori, *Adv. Opt. Mater.*, 2022, **10**, 2200864.

108 X. Kang, S. Wang, Y. Song, S. Jin, G. Sun, H. Yu and M. Zhu, *Angew. Chem., Int. Ed.*, 2016, **55**, 3611.

109 X. Kang, X. Li, H. Yu, Y. Lv, G. Sun, Y. Li, S. Wang and M. Zhu, *RSC Adv.*, 2017, **7**, 28606.

110 D. Arima, Y. Niihori and M. Mitsui, *J. Mater. Chem. C*, 2022, **10**, 4597.

111 M. Zhou, S. Jin, X. Wei, Q. Yuan, S. Wang, Y. Du and M. Zhu, *J. Phys. Chem. C*, 2020, **124**, 7531.

112 D. Arima and M. Mitsui, *J. Am. Chem. Soc.*, 2023, **145**, 6994.

113 R. Jin, C. Liu, S. Zhao, A. Das, H. Xing, C. Gayathri, Y. Xing, N. L. Rosi, R. R. Gil and R. Jin, *ACS Nano*, 2015, **9**, 8530.

114 L. Luo, Z. Liu, X. Du and R. Jin, *J. Am. Chem. Soc.*, 2022, **144**, 19243.

115 M. Bodiuzzaman, E. Khatun, K. S. Sugi, G. Paramasivam, W. A. Dar, S. Antharjanam and T. Pradeep, *J. Phys. Chem. C*, 2020, **124**, 23426.

116 Y. Niihori, S. Hossain, B. Kumar, L. V. Nair, W. Kurashige and Y. Negishi, *APL Mater.*, 2017, **5**, 053201.

117 A. Domínguez-Castro, C. R. Lien-Medrano, K. Maghrebi, S. Messaoudi, T. Frauenheim and A. Fihey, *Nanoscale*, 2021, **13**, 6786.

118 M. S. Devadas, K. Kwak, J.-W. Park, J.-H. Choi, C.-H. Jun, E. Sinn, G. Ramakrishna and D. Lee, *J. Phys. Chem. Lett.*, 2010, **1**, 1497.

119 R. Ho-Wu, K. Sun and T. Goodson, III, *J. Phys. Chem. C*, 2018, **122**, 2315.

120 W. Suzuki, R. Takahata, Y. Chiga, S. Kikkawa, S. Yamazoe, Y. Mizuhata, N. Tokitoh and T. Teranishi, *J. Am. Chem. Soc.*, 2022, **144**, 12310.

121 K. G. Thomas and P. V. Kamat, *Acc. Chem. Res.*, 2003, **36**, 888.

122 K. Konishi, M. Iwasaki, M. Sugiuchi and Y. Shichibu, *J. Phys. Chem. Lett.*, 2016, **7**, 4267.

123 M. Iwasaki, Y. Shichibu and K. Konishi, *Angew. Chem., Int. Ed.*, 2019, **58**, 2443.

124 M. Sugiuchi, Y. Shichibu, T. Nakanishi, Y. Hasegawa and K. Konishi, *Chem. Commun.*, 2015, **51**, 13519.

125 Y. Negishi, U. Kamimura, M. Ide and M. Hirayama, *Nanoscale*, 2012, **4**, 4263.

126 K. Pyo, N. H. Ly, S. M. Han, M. B. Hatshan, A. Abuhagr, G. Wiederrecht, S.-W. Joo, G. Ramakrishna and D. Lee, *J. Phys. Chem. Lett.*, 2018, **9**, 5303.

127 T. Saegusa, H. Sakai, H. Nagashima, Y. Kobori, N. V. Tkachenko and T. Hasobe, *J. Am. Chem. Soc.*, 2019, **141**, 14720.

128 M. M. Mitchell, V. W. Liyana Gunawardana, G. Ramakrishna and G. Mezei, *ACS Omega*, 2021, **6**, 33180.

129 Y. Niihori, K. Yoshida, S. Hossain, W. Kurashige and Y. Negishi, *Bull. Chem. Soc. Jpn.*, 2019, **92**, 664.

130 Y. Niihori, Y. Koyama, S. Watanabe, S. Hashimoto, S. Hossain, L. V. Nair, B. Kumar, W. Kurashige and Y. Negishi, *J. Phys. Chem. Lett.*, 2018, **9**, 4930.

131 Y. Niihori, D. Shima, K. Yoshida, K. Hamada, L. V. Nair, S. Hossain, W. Kurashige and Y. Negishi, *Nanoscale*, 2018, **10**, 1641.

132 Y. Niihori, Y. Kikuchi, A. Kato, M. Matsuzaki and Y. Negishi, *ACS Nano*, 2015, **9**, 9347.

133 Y. Niihori, M. Matsuzaki, T. Pradeep and Y. Negishi, *J. Am. Chem. Soc.*, 2013, **135**, 4946.

134 L. G. AbdulHalim, M. S. Bootharaju, Q. Tang, S. Del Gobbo, R. G. AbdulHalim, M. Eddaoudi, D.-E. Jiang and O. M. Bakr, *J. Am. Chem. Soc.*, 2015, **137**, 11970.

135 A. Ghosh, D. Ghosh, E. Khatun, P. Chakraborty and T. Pradeep, *Nanoscale*, 2017, **9**, 1068.

136 X. Kang, S. Wang and M. Zhu, *Chem. Sci.*, 2018, **9**, 3062.

137 Y. Niihori, N. Takahashi and M. Mitsui, *J. Phys. Chem. C*, 2020, **124**, 5880.

138 E. Khatun, A. Ghosh, P. Chakraborty, P. Singh, M. Bodiuzzaman, P. Ganesan, G. Nataranjan, J. Ghosh, S. K. Pal and T. Pradeep, *Nanoscale*, 2018, **10**, 20033.